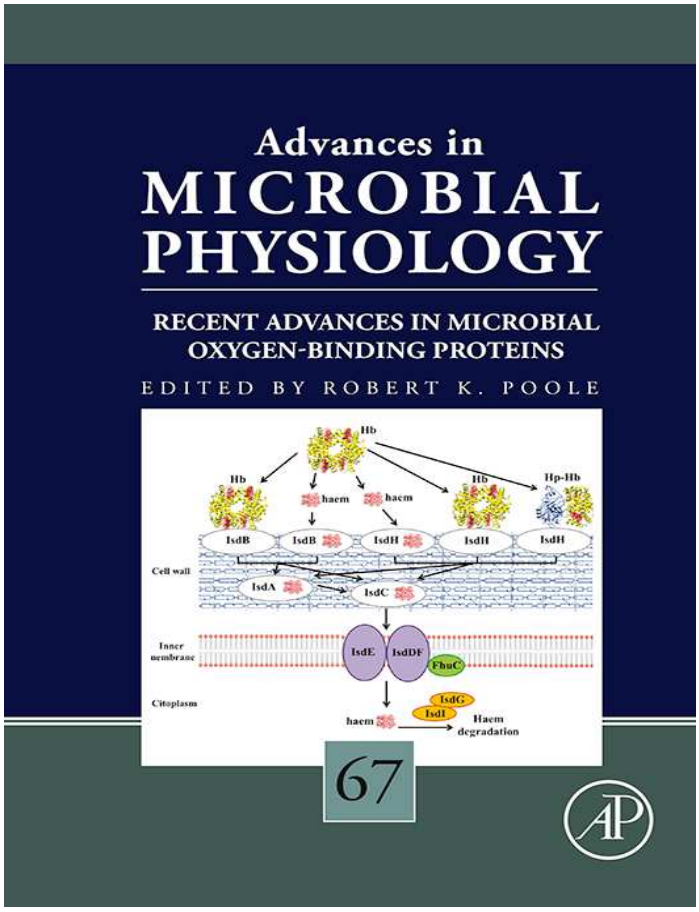

From Barry D. Howes, Leonardo Boechi, Alberto Boffi, Dario E. Estrin and Giulietta Smulevich, Bridging Theory and Experiment to Address Structural Properties of Truncated Haemoglobins: Insights from *Thermobifida fusca* HbO. In: Robert K. Poole, editor, *Advances in Microbial Physiology, Vol. 67*, Oxford: Academic Press, 2015, pp. 85-126.
ISBN: 978-0-12-803298-5

CHAPTER TWO

Bridging Theory and Experiment to Address Structural Properties of Truncated Haemoglobins: Insights from *Thermobifida fusca* HbO

Barry D. Howes*, Leonardo Boechi†, Alberto Boffi‡, Dario E. Estrin§, Giulietta Smulevich*,1

*Dipartimento di Chimica "Ugo Schiff", Università di Firenze, Sesto Fiorentino, Italy
†Instituto de Cálculo, Facultad de Ciencias Exactas y Naturales, Universidad de Buenos Aires, Ciudad Universitaria, Buenos Aires, Argentina
‡Dipartimento di Scienze Biochimiche, Università "Sapienza", Rome, Italy
§Departamento de Química Inorgánica, Analítica y Química Física and Inquimae-Conicet, Facultad de Ciencias Exactas y Naturales, Universidad de Buenos Aires, Buenos Aires, Argentina
1Corresponding author: e-mail address: giulietta.smulevich@unifi.it

Contents

Abstract

In this chapter, we will discuss the paradigmatic case of *Thermobifida fusca* (Tf-trHb) HbO in its ferrous and ferric states and its behaviour towards a battery of possible ligands. This

Advances in Microbial Physiology, Volume 67
ISSN 0065-2911
http://dx.doi.org/10.1016/bs.ampbs.2015.08.002

choice was dictated by the fact that it has been one of the most extensively studied truncated haemoglobins, both in terms of spectroscopic and molecular dynamics studies. Tf-trHb typifies the structural properties of group II trHbs, as the active site is characterized by a highly polar distal environment in which TrpG8, TyrCD1, and TyrB10 provide three potential H-bond donors in the distal cavity capable of stabilizing the incoming ligands. The role of these residues in key topological positions, and their interplay with the iron-bound ligands, has been addressed in studies carried out on the CO, F^-, OH^-, CN^-, and HS^- adducts formed with the wild-type protein and a combinatorial set of mutants, in which the distal polar residues, TrpG8, TyrCD1, and TyrB10, have been singly, doubly, or triply replaced by a Phe residue. In this context, such a complete analysis provides an excellent benchmark for the investigation of the relationship between protein structure and function, allowing one to translate physicochemical properties of the active site into the observed functional behaviour. Tf-trHb will be compared with other members of the group II trHbs and, more generally, with members of the other trHb subgroups.

ABBREVIATIONS

5c 5 coordinate
6c 6 coordinate
Bs-HbO group II trHb from *Bacillus subtilis*
CCP cytochrome *c* peroxidase
CCP(MI) CCP expressed in *E. coli* containing Met-Ile at the N-terminus
Cj-trHbP group III trHb from *Campylobacter jejuni*
CT1 charge transfer transition $[a_{2u}(\pi) \rightarrow e_g(d\pi)]$
CT2 charge transfer transition $[a_{2u}(\pi) – a_{1g}(d_{z2})]$
DHP dehaloperoxidase
GCSs globin-coupled sensors
HbA tetrameric human Hb
HbI, HbII, HbIII haemoglobin I, II, and III from *Lucina pectinata*
hh horse heart
HRPC horseradish peroxidase isoenzyme C
HS high spin
LS low spin
Mb myoglobin
MD molecular dynamics
Mt-tHbN group I trHb from *Mycobacterium tuberculosis*
Mt-tHbO group II trHb from *Mycobacterium tuberculosis*
Pgbs protoglobins
RR resonance Raman
sw sperm whale
Tf-tHbO group II trHb from *Thermobifida fusca*
trHbs truncated haemoglobins

1. INTRODUCTION

1.1 Microbial Haemoglobins

The first observation of haemoglobins (Hbs) in microorganisms was made by Warburg in the 1930s and thoroughly reported 20 years later by Keilin, who spectroscopically assigned oxygen-dependent Hb-like absorption bands in moulds, fungi, and protozoa (Keilin, 1953). Many years later, Hbs were also demonstrated to be present in bacteria (Wakabayashi, Matsubara, & Webster, 1986) and most recently even in archaea (Freitas et al., 2004). Phylogenetic analysis of protein sequences has indicated that globins are present in all kingdoms of life and can be collected within a single superfamily that contains three main lineages: (i) truncated haemoglobins (trHbs), (ii) protoglobins (Pgbs) and related globin-coupled sensors (GCSs), and (iii) flavohaemoglobins and related single-domain globins (Frey & Kallio, 2003; Vinogradov, Bailly, et al., 2013; Vinogradov & Moens, 2008; Wajcman, Kiger, & Marden, 2009; Wittenberg, Bolognesi, Wittenberg, & Guertin, 2002). Among these, classical vertebrate Hbs represent just a cluster within the last group of the globin superfamily. According to this view, O_2 transport, the hallmark of Hb function, appears as a recently emerged specialized trait associated with the evolution of metazoans (Pesce, Bolognesi, & Nardini, 2013). A survey of globin occurrence in bacterial and archaeal genomes revealed that over half of the bacterial and approximately one-fifth of archaeal genomes contain genes encoding for globins belonging to at least one of the three lineages (Vinogradov, Tinajero-Trejo, Poole, & Hoogewijs, 2013). A physiological role comprising nitric oxide detoxification via NO dioxygenase or denitrosylase activities and/or the sensing of gaseous ligands (oxygen, hydrogen sulphide, cyanide, etc.) in environmental niches has been suggested but it has been demonstrated only in a very few cases, notably for a few GCSs (Martínková, Kitanishi, & Shimizu, 2013). As such, the physiological function of most microbial globins still remains unknown. Structural biology data offer another multifaceted view of the globin superfamily and of microbial globins in particular. Members of the globin superfamily can be assigned to two main structural classes, one based on a 2-on-2 α-helical sandwich (trHbs) and the other showing the classical 3-on-3 α-helical motif (Pgbs and single-domain globins). The differences among the two diverse Hb folds are exemplified in

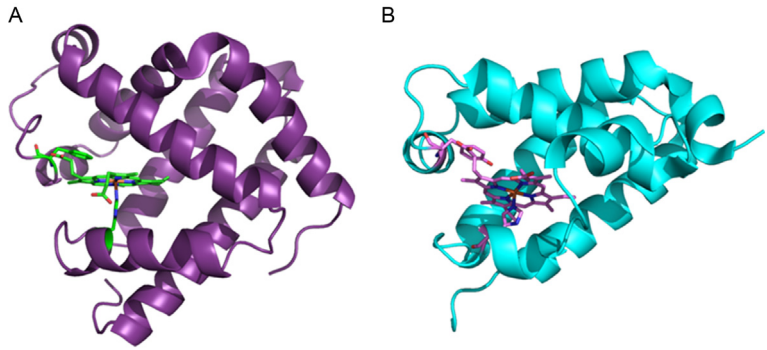

Figure 1 Comparison of the overall fold of a vertebrate globin and a truncated globin. (A) The eight-helix assembly of horse heart myoglobin (PDB code: 1MBN) is shown in magenta (dark grey in the print version); haem, with the HisF8 proximal ligand and PheCD1 is depicted in green (light grey in the print version). (B) The six-helix assembly of *Thermobifida fusca* truncated haemoglobin (PDB code: 2BMM) is shown in cyan (dark grey in the print version), haem, with HisF8 and TyrCD1 in pink (grey in the print version). The figure was prepared using Chimera software (UCSF Chimera).

Fig. 1 and highlight that, at variance with the eight-helix arrangement of classical globins, trHbs achieve a simplified 2-on-2 fold characterized by a very short or absent A-helix, a brief CE inter-helical region, the F-helix occurring as a loop with the B, E, G, and H regions surrounding the haem group. Thus, features common to all microbial Hbs are restricted to the presence of a proximal histidine at the F8 position that coordinates to the haem iron, and a tyrosine or phenylalanine residue at the CD1 position in the distal pocket, necessary for stabilizing the haem moiety in the pocket.

1.2 Truncated Haemoglobins

TrHbs are widely distributed in bacteria, archaea, and plants and are also found in some unicellular eukaryotes. They display less than 20% overall identity with respect to the 3-on-3 globins and can be conveniently classified into three groups, designated I (trHbN), II (trHbO), and III (trHbP). The overall sequence identity between trHbs from different groups may be as low as 20%, though it may be much higher within a given group (80%). Some bacteria display multiple trHbs belonging to different groups, thus suggesting the presence of an ancestor gene (possibly trHbO) that underwent duplications and transfer events during the evolutionary pathway (Pesce et al., 2013). From the structural point of view, each group displays specific features at the basis of distal pocket structure and polarity, as well as ligand stabilization and ligand entry/exit mechanisms. TrHbs share seven

key residues in the haem pocket at topologically relevant positions, namely B9, B10, CD1, E7, E11, E14, and F8. Nevertheless, besides HisF8, only PheB9 and TyrB10 are highly conserved and are thus thought to be of critical importance for ligand binding. Other topologically important positions in the haem pocket are not conserved and may vary in size and charge, thus changing completely the dielectric properties of the distal pocket. Such a profound diversity between trHbs might be associated with diverse functional properties concerned with ligand recognition and/or ligand affinity. However, it is noted that physiologically relevant activities such as gaseous ligand sensors, nitric oxide detoxification, and long-term ligand storage are presently not fully clarified. Nevertheless, *in vitro* experimental evidence does indicate diverse ligand-binding properties and complex ligand entry/exit dynamics that are characteristics of each group. Notable examples concern the unusually high affinity for cyanide in trHbP from *Campylobacter jejuni* (Cj-trHbP) (group III), the genuine peroxidase activity of trHbs from *Thermobifida fusca* (Tf-tHbO) and *Mycobacterium tuberculosis* (Mt-tHbO) (group II), or the distinctive NO dioxygenase capabilities identified in trHbNs (group I) (Arya et al., 2013; Ouellet, Milani, et al., 2007; Ouellet, Ranguelova, et al., 2007; Tinajero-Trejo & Shepherd, 2013; Torge et al., 2009).

2. AN OVERVIEW OF RESONANCE RAMAN SPECTROSCOPY OF HAEM PROTEINS

Over the past several decades, resonance Raman (RR) spectroscopy has been extensively applied to the study of structure, function, folding, and dynamics of haem proteins. In fact, it has a number of characteristics that have been advantageous in its application in the field of haem proteins (i) it requires only very small quantities of protein (samples are normally ~50 μL, 30–50 μM); (ii) it can be used easily for proteins in aqueous media, hence, reflecting physiological conditions, since the Raman water spectrum is very weak; and (iii) it is able to enhance only the vibrational modes of a chosen chromophore in proteins with multiple chromophores. There are many excellent reviews on the application of RR to haem proteins (Spiro, 1988), and recently, Yeh and co-workers have published two comprehensive reviews dedicated to trHbs (Egawa & Yeh, 2005; Lu, Egawa, Mukai, Poole, & Yeh, 2008).

In general, the combined analysis of electronic absorption and RR spectra enables some general conclusions to be obtained. The electronic

absorption spectrum is characterized by the $\pi \rightarrow \pi^*$ electronic transitions in the Soret (380–440 nm) and visible Q band (500–600 nm) regions deriving from the haem chromophoric group (Gouterman, 1978). In addition, high-spin (HS) ferric haem proteins show also weak bands assigned to porphyrin to iron charge transfer transitions [$a_{2u}(\pi)$–$a_{1g}(d_{z2})$] (CT2) and [$a_{2u}(\pi) \rightarrow e_g(d\pi)$] (CT1) in the 450–470 and 600–650 nm regions, respectively (Adar, 1978). When haem proteins are excited with a laser wavelength coincident with these electronic transitions, only the Raman spectrum of the haem moiety is enhanced (RR effect). In particular, excitation in the Soret and Q bands leads to the intensification of the haem vibrational modes, whereas by excitation in the CT bands Fe–ligand stretching modes are intensified (see below). Therefore, the haem active site can be probed and information on the structure–function relationship obtained.

2.1 Core-Size Marker Bands

In the high-frequency (1300–1700 cm^{-1}) spectral region, the skeletal modes, the so-called core-size marker bands, have been found to be sensitive to important aspects of porphyrin geometry and electronic structure. Many RR studies on haem proteins and model compounds have shown that their frequencies are inversely correlated with the size of the porphyrin core and, therefore, depend on the spin and coordination states of the Fe atom (Spiro & Li, 1988). Table 1 reports the expected frequencies for a number of more important core-size marker bands, determined by their sensitivity to

Table 1 Resonance Raman Frequencies (cm^{-1}) and Assignments for the Core-Size Marker Bands of Ferric and Ferrous Haem Proteins (Choi et al., 1982)[a]

	Spin State				
	Ferric			Ferrous	
Mode	6cHS	5cHS	6cLS	5cHS	6cLS
ν_4	1370	1373	1373	1357	1359
ν_3	1480	1491	1502	1471	1493
ν_{11}	1545	1553	1562	1547	1539
ν_2	1559	1570	1579	1562	1584
ν_{37}	1580	1591	1602	1550	1583
ν_{10}	1610	1626	1640	1604	1617

[a]6cHS, 6 coordinate high spin; 5cHS, 5 coordinate high spin; 6cLS, 6 coordinate low spin.

the coordination and spin state of the haem. The strong band between 1350 and 1380 cm^{-1}, assigned to the ν_4 mode, is sensitive to the π-electron density of the porphyrin macrocycle and, therefore, the oxidation state of the iron. The ν_3, ν_2, and ν_{10} modes, which give rise to bands in the 1475–1510, 1550–1590, and 1600–1640 cm^{-1} regions, respectively, are sensitive to both the axial coordination and spin state of the iron.

2.2 Fe–Ligand Modes

Interactions of ligands with the protein side chains that line the haem pocket are critical for discriminating among the binding of the various ligands, and for regulating the subsequent protein conformational changes or the ligand reactivity. Steric contacts can prevent ligand binding or induce slight distortions of the porphyrin ring geometry, thus modifying the Fe–ligand electronic properties. In addition, electric fields and H-bonds associated with side chains distal to the bound ligand can polarize the Fe–ligand bond. The characterization of these interactions is fundamental in order to understand the underlying physical and chemical properties of haem protein functions. In this framework, vibrational spectroscopy offers a powerful tool since in the low-frequency region of the RR spectrum, the Fe–ligand stretching vibrations can be detected. Their frequency is strongly modulated by the interactions between the ligand and the surrounding amino acids (see below); therefore, information on the role of the haem cavity residues in ligand stabilization and the hydrogen-bonding network lining the proximal and distal sides of the haem can be obtained.

The frequencies of specific iron–ligand modes are typically located in the 200 and 800 cm^{-1} frequency region of the RR spectrum and are intensified with excitation in the Soret and/or CT bands (Droghetti et al., 2011; Kerr & Yu, 1988; Spiro, 1988). The haem protein ferric derivatives of a variety of small molecules, such as H_2O, NO, CN^-, H_2S, and F^-, have been identified. The most frequently studied ferrous haem ligands are oxygen-containing diatomic molecules, such as O_2, CO, and NO. Moreover, the RR band associated with the iron–histidine stretching mode has been observed only in the five-coordinate ferrous derivatives (Kitagawa, 1988).

2.2.1 The Proximal Iron–Histidine Stretching Mode

The Fe–His bond stretching mode, ν(Fe–His), is an optimum probe of the proximal cavity structure as it is very sensitive to the protein matrix, its frequency being strongly affected by the H-bonds between the N_δ atom of the proximal His and nearby residues (Kitagawa, 1988; Stein, Mitchell, & Spiro,

1980; Teraoka & Kitagawa, 1980). In the case of a proximal ligand containing a neutral His, the ν(Fe–His) mode has been found at around 200 cm^{-1}, while deprotonation at the N_δ position increases the frequency to the region between 240 and 260 cm^{-1}. Such up-shifted frequencies are typical of haem-containing peroxidases, which have an imidazolate ligand resulting from the strong H-bonding interaction between the proximal His and a nearby carboxylate group of an Asp residue (Smulevich, Feis, Howes, & Ivancich, 2010). In myoglobin (Mb), where the N_δ proton is H-bonded to a neutral backbone carbonyl group, the ν(Fe–His) stretch was found at 220 cm^{-1} (Kitagawa, Nagai, & Tsubaki, 1979), while in the tetrameric human Hb (HbA) the frequency shifts to 214 cm^{-1} since the iron–histidine bond is strained by the F-helix due to the T-state quaternary interactions (Hori & Kitagawa, 1980; Kitagawa, 1988; Spiro & Li, 1988).

2.2.2 The Distal Ligands

A key objective of the characterization of haem proteins is to establish well-defined correlations between functional aspects and chemical properties of the active site. In general, the reactivity of the active site depends on the oxidation and spin state of the iron ion, the status of the proximal iron ligand, and the nature of the distal cavity residues. In particular, the distal protein amino acids can stabilize (or destabilize) the iron-bound ligands through a manifold of interactions. H-bonds play a significant role in determining ligand stabilization, and different interactions can be envisaged, e.g., single residue-to-ligand H-bonds (Streit, Blanc, Lukat-Rodgers, Rodgers, & DuBois, 2010), water-mediated H-bonds (Edwards & Poulos, 1990), or even ligand inclusive H-bond networks (Egawa & Yeh, 2005; Feis et al., 2008; Ouellet et al., 2003; Rodriguez, Zeng, Wilks, & Rivera, 2007).

In general, the metal–ligand stretching modes can be selectively enhanced by tuning the laser frequency within the Soret or charge transfer transition bands (CT1 or CT2) (Kerr & Yu, 1988; Spiro, 1982). The nature and sensitivity of the metal–ligand bond to the haem structure and haem environment make the frequency of these stretching modes an ideal probe able to provide detailed information on the haem–ligand–protein interactions.

2.2.2.1 H_2O/OH^-

Water is the most common ligand for ferric haem proteins, giving rise to a 6cHS aquo-met derivative with an axially coordinated water ligand in the distal position. The ν(Fe–H_2O) stretching mode, however, has never been

observed in the RR spectrum of any haem protein due to its weak intensity. At alkaline pH, the majority of haem proteins undergo an acid–alkaline transition, characterized by a hydroxide ligand bound to the haem iron. The ν(Fe–OH) stretching frequency is very sensitive to the distal environment. An increase of the H-bond strength between the hydroxo group and nearby proton donor/acceptor residues determines a decrease of the force constant of the Fe–OH^- bond with the concomitant decrease of the ν(Fe–OH) stretching frequency.

In Mb and HbA, the haem-bound hydroxide group is stabilized by a weak H-bond with the distal His residue, and two ν(Fe–OH) modes have been observed at about 490 and 550 cm^{-1}. They correspond to the six coordinate HS and low-spin (LS) species, respectively (Feis, Marzocchi, & Smulevich, 1994). In contrast, in haem-containing peroxidases, where both the distal Arg and His residues are involved in a concerted manner via H-bonds in the stabilization of the ligand, the haem-bound hydroxide gives rise to a 6cLS haem, with a ν(Fe–OH) frequency around 500 cm^{-1} (Feis et al., 1994; Howes, Feis, Indiani, Marzocchi, & Smulevich, 2000; Howes, Rodriguez-Lopez, Smith, & Smulevich, 1997; Nissum, Feis, & Smulevich, 1998; Sitter, Shifflett, & Terner, 1988). This frequency is about 50 cm^{-1} wavenumbers lower than that observed in the globins, confirming the presence of strong H-bonds. These results clearly show the high sensitivity of the ν(Fe–OH) frequency to the distal environment.

2.2.2.2 Fluoride

Another ligand that recently has attracted attention as a probe of the H-bonding interaction between the ligand and the distal cavity is fluoride. Fluoride is an anionic weak-field ligand that coordinates ferric haems at pH values below 7.0, with the formation of a 6cHS complex. These complexes are characterized by a strong Soret band with maxima between 404 and 406 nm and a weak Q band at 490 nm. In addition, the electronic absorption spectrum displays an interesting feature in the 600–620 nm range, where a weak band due to a charge transfer transition (CT1) appears. Its wavelength is a sensitive probe of axial ligand polarity and of its interaction with the distal protein residues. It has been found that it blue-shifts when the p- and/or π-donor capability of the axial ligand increases or when the ligand acts as a H-bond donor (e.g. H_2O or H_3O^+), since the interaction between the p/π orbitals of the ligand and the iron dπ orbitals raises the energy of the latter (Smulevich, Neri, Marzocchi, & Welinder, 1996; Smulevich et al., 1997). The opposite effect is observed when the ligand acts as an H-bond

acceptor, as in the case of the fluoride ligand (Neri, Kok, Miller, & Smulevich, 1997). In particular, an extensive study on haem peroxidases from various organisms suggested that the position of the CT1 maximum could be related to structural properties of the protein cavity surrounding the bound fluoride anion, demonstrating the sensitivity of the fluoride ligand to the distal cavity environment. For example, distal mutations markedly affected the CT1 position of the fluoride complex of cytochrome *c* peroxidase (CCP). In particular, the CT1 maximum observed at 617 nm as a result of three H-bonds donated to the fluoride by Arg48, Trp51, and a water molecule, blue-shifted in the W51F mutant where replacement of the distal Trp by a non-H-bonding Phe residue reduces the number of H-bonds of the ligand with the protein matrix from three to two. This confirmed that when a ligand acts as a hydrogen-bond donor, the stronger the hydrogen bond and the charge donation to the iron atom, the lower is the wavelength of the CT1 band.

In addition to the UV–vis spectra, the RR frequency of the ν(Fe–F) stretching mode in the low-frequency region provides direct evidence for H-bonding of the fluoride ligand to distal residues via information on the Fe–ligand strength. In fact, the ν(Fe–F) stretching frequency is directly affected by H-bonding to the fluoride ion. This is mainly due to the reduction of the Fe–F bond strength in H-bonded complexes, as a consequence of a decreased electron density on the fluoride ion. The ν(Fe–F) stretching modes appear in the region between 370 and 470 cm^{-1}. In Mb, at neutral pH, a band at 462 cm^{-1} has been assigned to a Fe–F stretching mode on the basis of the 2 cm^{-1} up-shift observed upon $^{56}Fe/^{54}Fe$ isotopic substitution (Desbois, Lutz, & Banerjee, 1979). A clear correlation between the absorption maxima of the CT1 and the H-bonding to the bound anion has been found, thus indicating that fluoride is a sensitive probe of the distal environment in peroxidases (Neri et al., 1997). Moreover, a low ν(Fe–F) stretching frequency has been shown to correlate with a red-shifted CT1 band in the complexes where fluoride is strongly H-bonded to distal pocket residues.

2.2.2.3 H_2S

Hydrogen sulphide, a well-known poisonous gas, is emerging as the fourth (together with O_2, NO, and CO) gas molecule which can act as a signal for intermolecular transduction. In fact, the discovery that H_2S is produced naturally in the human body has changed the perception of this molecule from a toxic pollutant to a biologically relevant molecule (Pietri, Roman-Morales, & Lopez-Garriga, 2011).

Interaction of H_2S with the haem iron is very complex due to the high reactivity of the molecule and many diverse reactions have been observed. It has been known for a long time that the reaction of excess H_2S with metMb or metHb in the presence of O_2 forms a green derivative, as a consequence of the formation of a sulphhaem complex in which the sulphur atom is inserted within the macrocycle ring (Keilin, 1933; Nicholls, 1961; Ríos-Gonzalez, Roman-Morales, Pietri, & Lopez-Garriga, 2014). In addition, in haem proteins, residues from the proximal (Bieza et al., 2015) and distal sides (Ríos-Gonzalez et al., 2014) of the haem cavity appear to modulate the reactivity of the haem group, since some haem proteins have been found to be reduced by sulphides (Hill & Nicholls, 1980; Nicoletti, Thompson, Franzen, & Smulevich, 2011; Pietri et al., 2009), whereas others form remarkably stable FeIII–S(sulphide) adducts (Boffi, Rizzi, Monacelli, & Ascenzi, 2000; Nicoletti et al., 2010).

Interestingly, the HS^- anion has recently been suggested to be a potential physiological ligand for haem proteins. A wide range of organisms have been suggested to be involved in such a mechanism from bacteria, e.g., the trHbs from *B. subtilis* and *T. fusca* (Nicoletti et al., 2010), to marine invertebrates living in sulphide-rich environments, such as the clam Hb of *Lucina pectinata* (Bailly & Vinogradov, 2005; Kraus & Wittenberg, 1990), and dehaloperoxidase-haemoglobin (DHP), an enzyme isolated from the marine worm *Amphitrite ornata*, that serves as the respiratory Hb and has a detoxification function for the organism (Nicoletti, Thompson, et al., 2011). Sulphide binding to these ferric proteins resulted in the formation of a 6cLS complex with a typical electronic absorption spectrum characterized by a Soret maximum at about 424–427 nm and a RR ν(Fe–S) stretching mode around 375 cm^{-1} (Cerda, Echevarria, Morales, & Lopez-Garriga, 1999; Nicoletti et al., 2010; Nicoletti, Thompson, et al., 2011).

2.2.2.4 O_2

Among the various ligands which bind the haem iron in its ferrous state, the most extensively studied have been oxygen-containing diatomic molecules (X–O), such as O_2, CO, and NO (Spiro, Soldatova, & Balakrishnan, 2013). In fact, the function of many haem globin proteins is the transport of O_2 (Jensen, 2009). The first identification of the RR iron–dioxygen ν(Fe–O_2) stretching mode was in the RR spectrum of HbA in erythrocytes by Brunner in 1974 (Brunner, 1974). The ν(Fe–O_2) stretching mode has now been identified for several O_2-bound haem proteins by RR spectroscopy. In oxyMb and oxyHb, the ν(Fe–O_2) vibration has been identified, on

the basis of the $^{16}O_2$ and $^{18}O_2$ isotopic substitution experiments, around 570 cm^{-1} (Duff, Appelman, Shriver, & Klots, 1979; Hirota et al., 1996; Nagai, Kitagawa, & Morimoto, 1980). The X-ray structure of MbO_2 revealed that the haem-bound dioxygen is stabilized by the E7 His through H-bonding interactions to both oxygen atoms of the dioxygen. Unlike globins, trHbs are not oxygen transporters as they are not capable of fast oxygen delivery. Their very low rates of oxygen release are in fact a consequence of strong H-bonding interactions between the haem-bound O_2 and the amino acid residues lining the distal haem pocket; hence, the oxygen atom is tightly bound to the haem (Arroyo Mañez et al., 2011; Giangiacomo, Ilari, Boffi, Morea, & Chiancone, 2005; Ouellet et al., 2003). Therefore, in general, a very slow O_2 off-rate has been measured together with a very low ν(Fe–O_2) stretching frequency (Egawa & Yeh, 2005). For example, the ν(Fe–O_2) frequency of trHb-I from the green algae *C. eugametos* has been observed at 554 cm^{-1} (Das, Couture, Ouellet, Guertin, & Rousseau, 2001), in trHb-I from the eubacterium *M. tuberculosis* at 560 cm^{-1} (Couture et al., 1999), in Mt-trHbO(trHb-III) at 559 cm^{-1} (Mukai, Savard, Ouellet, Guertin, & Yeh, 2002), and in Cj-trHbP(trHb-III) at 542 cm^{-1} (Arroyo Mañez et al., 2011).

2.2.2.5 CO

While the function of many haem proteins is the transport of O_2 and NO, including globins (Jensen, 2009), the CO adduct has been used extensively as a probe of the nature and architecture of the haem-binding pocket, which can determine the reactivity of the haem towards other ligands, particularly O_2 and NO. Since the FeCO back-bonding is modulated by polar interactions and, in particular, by the formation of H-bonds between the bound CO and the distal protein residues (Spiro & Wasbotten, 2005), the electrostatic interaction between the FeCO unit and the protein alters the electron distribution in the FeCO unit with the consequent change of the order of the C–O bond. A positively charged electrostatic field favours back-donation, which strengthens the Fe–C bond and correspondingly weakens the C–O bond, thereby increasing the ν(FeC) vibrational frequencies and decreasing the ν(CO) frequencies (Phillips, Teodoro, Li, Smith, & Olson, 1999). On this basis, an inverse linear correlation has been established between the frequencies of the ν(FeC) and ν(CO) stretching modes for a large class of haem protein CO complexes containing imidazole as the fifth iron ligand, the most common proximal ligand in haem proteins (Kerr & Yu, 1988) (see Fig. 2). The ν(FeC)/ν(CO) position along the correlation

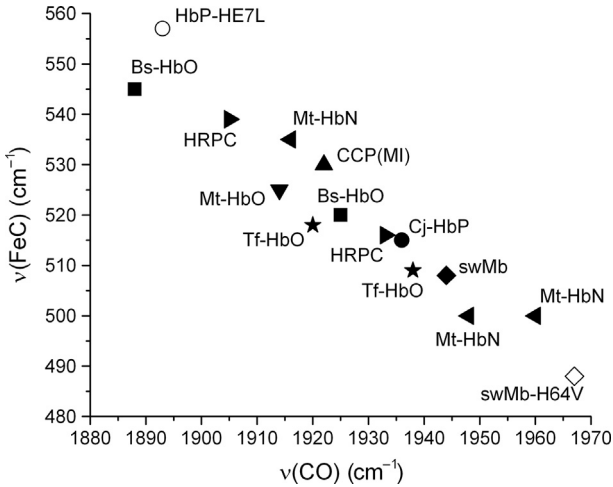

Figure 2 Back-bonding correlation plot for the ν(Fe–C) and ν(C–O) stretching frequencies of various truncated Hbs, peroxidases, and Mb: Bs-HbO (■), Mt-HbO (▼), Tf-HbO (★), Mt-HbN (◄), Cj-HbP (●) and its HE7L mutant (○), HRPC (►), CCP(MI) (▲), and sperm whale (sw) Mb (◆) and its H64V mutant (◇). The data points and corresponding references are reported in Table 2.

line reflects the type and strength of distal polar interactions (Spiro & Wasbotten, 2005), as clearly shown by the CO adducts of a series of Mb distal variants (Phillips et al., 1999). The calculated electrostatic potential field distributions of the bound CO in the distal pockets correlate inversely with ν(C–O) and directly with ν(Fe–CO). The distal histidine residue (H64) of wild-type (WT) Mb forms a weak H-bond interaction with the bound CO, resulting in a point located in the central region of the back-bonding line. When the distal histidine is replaced by hydrophobic residues (e.g. H64V), the ν(FeC)/ν(CO) point slides down the line reflecting the expected decreased back-bonding. On the contrary, proteins with distal residues that strongly interact with the bound CO via H-bonds lie higher on the line, as shown by horseradish peroxidase (HRPC) and recombinant CCP [CCP (MI)] and a series of Hbs from all three classes of trHbs (Fig. 2, Table 2). In fact, peroxidases and trHbs, which are both characterized by polar distal cavities, display similar CO-binding properties. A comparison between the CO binding in globins and peroxidases clearly indicates that back-donation is stronger in peroxidases than in globins. Studies involving site-directed mutagenesis to trace the distal interactions with CO have demonstrated that in peroxidases, the distal arginine and histidine residues that play critical roles in peroxide activation form strong H-bonds with the bound CO. As a

Table 2 Vibrational Frequencies (cm^{-1}) of the CO Complexes of Various Truncated Hbs, Peroxidases, and Mb

Protein	ν(Fe–C)	ν(C–O)	Reference
Truncated Hb Class I			
M. tuberculosis HbN	535	1916	Samuni, Ouellet, Guertin, Friedman, and Yeh (2004)
	500	1948	
	500	1960	
Truncated Hbs Class II			
B. subtilis HbO	545 (form 1)	1888	Feis et al. (2008)
	520 (form 2)	1925	
M. tuberculosis HbO	525	1914	Mukai et al. (2002)
T. fusca HbO	518 (form 1)	1920	Droghetti et al. (2010)
	509 (form 2)	1938	
Truncated Hbs Class III			
C. jejuni HbP	515	1936	Wainwright, Wang, Park, Yeh, and Poole (2006) and Lu, Egawa, Wainwright, Poole, and Yeh (2007)
C. jejuni HbP-HE7L	557	1893	
Peroxidases			
HRPC	539 (form 1)	1905	Feis, Rodriguez-Lopez, Thorneley, and Smulevich (1998), Uno et al. (1987), and Evangelista-Kirkup, Smulevich, and Spiro (1986)
	516 (form 2)	1933	
CCP(MI)	530	1922	Smulevich, Evangelista-Kirkup, English, and Spiro (1986)
Mb			
swMb	508	1944	Li, Quillin, Philips, and Olson (1994), Tsubaki, Srivastava, and Yu (1982), and Howes, Helbo, Fago, and Smulevich (2012)
swMb H64V	488	1967	Li et al. (1994) and Ling, Li, Olson, and Bocian (1994)

consequence, their ν(FeC)/ν(CO) points lie in the upper left corner of the correlation line (Smulevich, Feis, & Howes, 2005).

3. COMPUTER SIMULATION TECHNIQUES

Computer simulation techniques to model biomolecular systems have emerged during the last few decades as an important tool to complement experimental studies (Karplus & McCammon, 2002). The *in silico* generated models and the information that can be obtained through their study have proven to be essential for analysing the structural, spectroscopic, and kinetic data provided by experimental methods (Elber, 2010).

In particular, computer simulations allow a systematic and economical tool to analyse the dependence of a property of interest on static (e.g. amino acid sequence) and dynamic factors. In recent years, the increase in computing power and the accuracy of the models have made it possible to draw biologically relevant conclusions and propose new hypotheses based mainly on computer-generated data (Guallar & Wallrapp, 2011; Norberg & Nilsson, 2002; Roux & Schulten, 2004; Zhao & Caflisch, 2015). The hydrogen-bond network of trHbs is dynamic and several conformations should be considered; consequently, molecular dynamics (MD) simulations emerge as a very important tool for studying the active site of haem proteins. It is important to note that the dynamical features of the active sites of trHbs do not involve the formation or breaking of chemical bonds, and thus, they can be modelled by using classical force fields. Such force fields require parameters that should be obtained by careful quantum-mechanical calculations.

During the last decade, our group has studied several haem proteins using MD simulations (Arroyo Mañez et al., 2011; Bidon-Chanal et al., 2006; Boechi et al., 2008; Forti et al., 2011). Herein, we focus our attention on the interactions between distal site residues and the ligand (O_2, CO, F^-, SH^-, OH^-) coordinated to the haem iron of trHbs. The hydrogen-bond network formed by all those actors, and especially their dynamical properties, allow us to address the molecular basis of protein behaviour towards these ligands, and thus to propose possible protein functions. Furthermore, comparison of single point mutants performed *in silico* also allows the determination of individual residue contributions to ligand affinity. Moreover, the combination of this kind of computer simulation with the previously described spectroscopic techniques constitutes a powerful approach to achieve a better understanding of the active sites of haem proteins.

The natural ligand of many haem proteins is the oxygen molecule, which adopts a negative charge density when coordinated to the iron of the haem group due to the significant charge transfer (π-back-bonding) from the haem group to the ligand. Thus, the coordinated oxygen is stabilized by polar distal site residues able to act as H-bond donors (Capece et al., 2013). Other ligands interact to a greater or lesser extent with the distal site residues depending on the charge density of the iron coordinated species.

4. *THERMOBIFIDA FUSCA* HB

The trHb from *T. fusca* (Tf-trHb) is an archetypal trHb in that it exemplifies the structural properties of group II trHbs (Bonamore et al., 2005). Interestingly, the presence of a gene coding for the Tf-trHb coexists with at least three different globin genes, including a gene encoding for a Pgb. Tf-trHb, similar to the highly homologous mycobacterial Mt-trHbO and *Bacillus* Bs-trHbO, is characterized by a very high affinity for oxygen, a significant NO dioxygenase activity, and a surprisingly high peroxidase-like activity. Besides these notable enzymatic properties, its role within the physiology of the microorganism has not been clarified.

Structure-based sequence alignments show unambiguously that Tf-trHb is closely related to Mt-trHbO and Bs-trHbO (Bonamore et al., 2005). The overall fold of Tf-trHb conforms to that of the other two group II Hbs, for which the X-ray structures are available: Mt-trHbO (PDB code: 1NGK) (Milani et al., 2003) and Bs-trHb (PDB code: 1UX8) (Giangiacomo et al., 2005). Comparison of the crystal structure of Tf-trHb with Bs-trHbO and Mt-trHbO indicates that there is a notable correspondence regarding the amino acids that constitute the haem pocket as discussed below.

4.1 Haem Cavity Structure

Distal haem pocket residues in the key topological positions that govern ligand-binding properties (PheB9, TyrB10, TyrCD1, AlaE7, LeuE11, and TrpG8) are all conserved in Tf-trHb and Mt-trHbO, whereas the key residue TyrB10 is substituted by a Phe residue in Bs-trHbO.

The potentially important role of these polar residues in ligand stabilization and the unique architecture of the active site of Tf-trHb, and other globins belonging to the same family, has stimulated extensive studies aimed at understanding the interplay between iron-bound ligands and distal amino acids. X-Ray crystallography has provided fundamental snapshots of the

active site structural framework and highlighted the network of interactions that contributes to modulate the functional properties of the macromolecule around the metal-binding site (Bonamore et al., 2005; Giangiacomo et al., 2005; Milani et al., 2003). On the basis of X-ray diffraction data and static or dynamic spectroscopic observations, it is now clear that iron-bound ligands in the haem-binding pocket experience a network of electrostatic fields and hydrogen-bonding interactions exerted by nearby amino acid side chains. In fact, specific short-range amino acid side chain interactions with ligands appear to contribute to the diversity of haem protein functional behaviour at a level of structural detail that is not always achievable even with high-resolution crystallographic data. Moreover, even if the crystal structure of a given protein is available, it is typically limited to a specific oxidation and coordination state, usually the resting state with no ligand in the distal cavity.

Therefore, a spectroscopic approach, using UV–vis, RR, FTIR, EPR, and/or NMR, complements the crystallographic studies. These techniques are helpful in revealing the dynamic nature of Hbs under various physical and chemical conditions. Among these spectroscopic tools, RR spectroscopy is especially versatile and informative. Combined with mutagenesis studies and MD simulations, RR has uncovered important structural features of several Hbs from unicellular organisms (Egawa & Yeh, 2005; Lu et al., 2008).

5. SPECTROSCOPY AND COMPUTER SIMULATION OF TF-trHb

5.1 Ferric

The UV–vis and RR spectra of the ferric derivative at neutral pH shows a mixture of 6cLS and 6cHS configurations, characteristic of a Fe–OH^- haem (UV–vis maxima at 541 and 577 nm) and a 6cHS aquo form (CT1 bands around 498 and 634 nm, respectively). Classical MD simulations reveal that the coordinated water is stabilized by strong H-bonds with the indole N proton of WG8 (H_2O–N_{WG8} = 1.9 Å) and the hydroxylic hydrogen of YCD1 (OH_2O–O_{YCD1} = 1.5 Å), confirming the spectroscopic findings that suggest a Fe–OH^- character of the ligand even at pH 6.1 (Nicoletti et al., 2014, 2013) (Fig. 3A).

The contribution from the LS component increases as the pH is raised, reflecting the complete deprotonation of the haem-bound water and the formation of a hydroxide derivative. In the RR spectrum at pH 9.8,

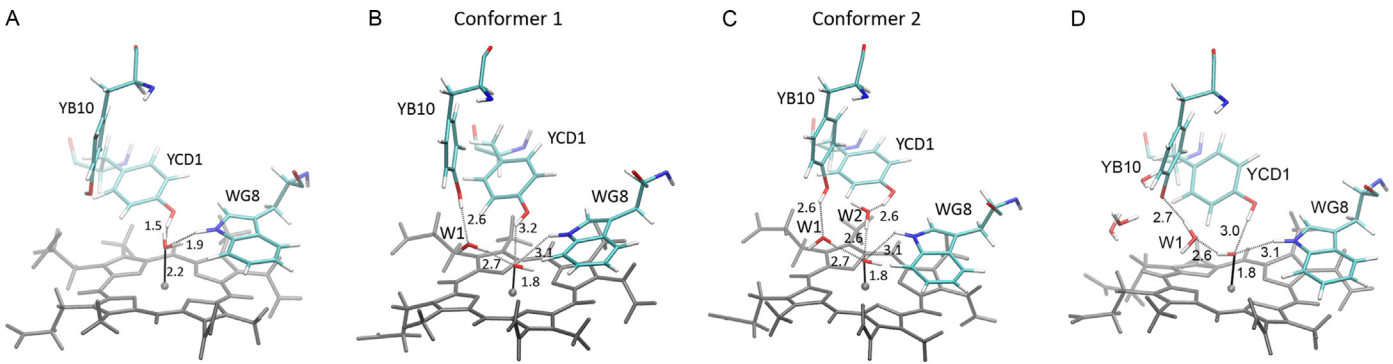

Figure 3 Schematic representation of the distal side of wild-type (WT) Tf-trHb at neutral (A) and alkaline pH (B–D). The dotted lines represent the hydrogen-bond network stabilizing the iron-bound H_2O (A) or the iron-bound OH^- in the two conformations of WT Tf-trHb at alkaline pH when both YB10 and YCD1 are protonated (B and C), or when only YB10 is deprotonated (D), on the basis of MD simulations. Distances are in angstroms.

a ν(Fe–OH) stretching mode has been observed at 485 cm^{-1} (Nicoletti et al., 2014, 2013). The remarkably low frequency, about 65 cm^{-1} lower than that observed for metMb and metHb (Feis et al., 1994), indicates the presence of strong multiple hydrogen bonds between the OH^- ligand and distal residues. In fact, with an increase of the H-bond strength, a decrease of the force constant of the Fe–OH^- bond with the concomitant decrease of the ν(Fe–OH) stretching frequency is expected. At alkaline pH, MD simulations show slightly different results depending on the protonation/deprotonation status of the distal YB10. When both tyrosines (YB10 and YCD1) were considered to be protonated, two conformations in which there is a strong hydrogen-bond network involving all three distal site residues and water molecules are obtained. In the first conformation, the coordinated anion is stabilized by direct interaction with TrpG8 and TyrCD1, and an indirect water-mediated interaction with TyrB10. In the second conformation, TyrCD1 and TyrB10 stabilize the coordinated anion by a water-mediated bridge (Nicoletti et al., 2013) (Fig. 3B and C). However, at extreme alkaline pH the tyrosines in the active site can be deprotonated, and thus, tyrosine becomes an hydrogen-bond acceptor modifying the hydrogen-bond network that stabilizes the coordinated anion (Nicoletti et al., 2014). Therefore, the MD simulations of the WT form containing a deprotonated YB10 residue show only one conformation. The OH^- ligand is acting as acceptor of direct H-bonds with TrpG8 and YCD1, whereas YB10 is H-bonded to one or two water molecules, one of which is H-bonded to the OH^- ligand as donor. This conformation is characterized by H-bonds that stabilize the OH^- ligand (Fig. 3D) more favourably than the case when both tyrosines are protonated (Fig. 3B and C).

Mutation of the distal residues with a Phe residue markedly affects the RR spectrum, resulting in an increased ν(Fe–OH) stretching frequency as a consequence of the change in the H-bond strength. The combined analysis of the RR and MD simulations clearly indicates (Fig. 4) that the singly mutated proteins show a similar, remarkable up-shift (between 20 and 28 cm^{-1}) of the ν(Fe–OH) frequency resulting from the rupture of one H-bond interaction. However, the strength of the H-bonding between the various distal residues and the hydroxo ligand is quite different, as highlighted by the different shift observed in the doubly mutated variants. The YB10F–YCD1F mutant, in which both distal Tyr residues are missing, behaves similar to the single mutants, whereas the YB10F–WG8F mutant, where the YCD1 is the only putative H-bond donor, shows a ν(Fe–OH) frequency comparable to that of WT, indicating a rearrangement of the

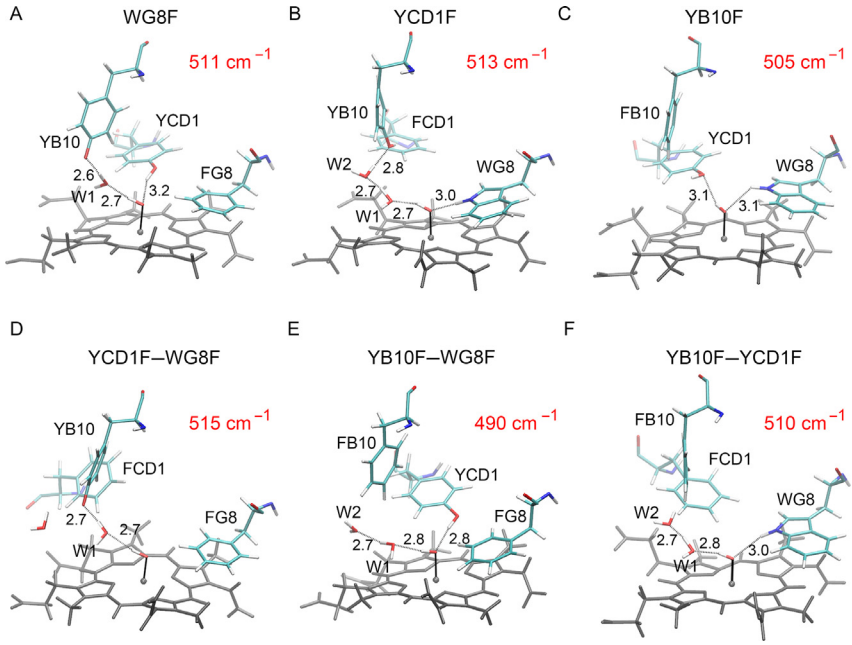

Figure 4 Schematic representation of the distal haem cavity of the mutated proteins at alkaline pH showing, on the basis of MD simulations, the hydrogen-bond network (dotted lines) stabilizing the iron-bound OH^- for single (A–C) and double (D–F) mutant proteins. As TyrB10 is deprotonated it acts as a H-bond acceptor, whereas WG8 and YCD1 are H-bond donors. Distances are in angstroms. The RR ν(Fe–OH) stretching mode frequencies for each mutant are shown in red. *Reprinted with permission from Nicoletti et al. (2014). Copyright (2014) American Chemical Society.*

residue and a strong H-bond interaction. In contrast, for the YCD1–WG8F mutant, where only YB10 can act as a potential H-bond donor, the highest frequency up-shift among all the variants is observed, thus indicating the weakest H-bond interaction to the hydroxo ligand among the three distal polar residues.

The behaviour described above for Tf-trHb is quite different from that observed for the group II Hb Mt-trHbO, for which a covalent bond between the phenyl oxygen of the TyrB10 and the Ce2 of the TyrCD1 is present in six subunits of the dodecamer. In the other six subunits, although the aromatic side-chain groups of the TyrB10 and TyrCD1 residues maintain a similar orthogonal orientation, they are only in very close contact but without the covalent linkage (Milani et al., 2003). This unique CD1/B10Tyr pair creates a tight and rigid distal environment for the incoming ligands. Consequently, while at neutral pH Mt-trHbO is a

mixture of HS and LS species, at pH 10.5 two ν(Fe–OH) modes were found at 446 and 533 cm^{-1} (Mukai et al., 2002). The 446 cm^{-1} mode disappeared when the TyrCD1 was mutated to Phe, while it was unchanged when the TyrB10 was mutated to Phe. Therefore, the 446 cm^{-1} mode has been associated with a conformation in which the haem-bound hydroxide is stabilized by an H-bond provided by the TyrCD1, but not the TyrB10. This scenario is consistent with the crystal structure of the ferric cyanide complex, in which the Fe-bound cyanide accepts H-bonds from the TyrCD1 and the TrpG8, but not from the TyrB10. The 533 cm^{-1} mode has been assigned to an open conformation in which the H-bonding interactions are absent (Mukai et al., 2002). In the TyrB10Phe or TyrCD1Phe mutant, the 533 cm^{-1} mode shifts to 510 cm^{-1}, presumably due to a reorganization of the distal pocket induced by the deletion of the covalent bond between the TyrB10 and the TyrCD1.

5.2 Ferrous

WT Tf-trHb and mutated proteins at pH 7.0 display electronic absorption Soret and Q bands (428–431 and 558 nm, respectively) and RR spectra typical of a 5cHS species (Droghetti et al., 2010). The ν(Fe–His) mode is at 223 cm^{-1}, intermediate between that of swMb (220 cm^{-1}) (Kitagawa et al., 1979) and that of other trHbs, like Mt-trHbO (226 cm^{-1}) (Samuni et al., 2004), and *Pseudoalteromonas haloplanktis* TAC125 trHbO (222 cm^{-1}) (Giordano et al., 2015, 2011). As for the latter proteins, the relatively short Fe–His bond can be ascribed to the staggered orientation of the imidazole plane of the proximal His with respect to the haem nitrogen atoms (see Fig. 5), in contrast to the eclipsed orientation in Mb and HbA (Droghetti et al., 2010; Samuni et al., 2004). Hence, the higher frequency

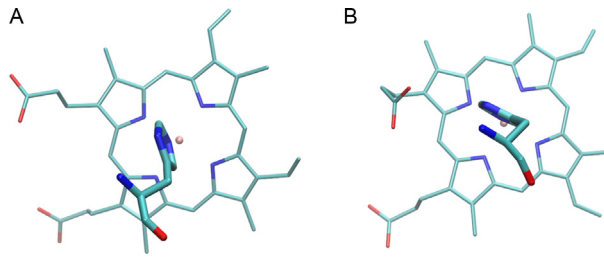

Figure 5 View of the proximal side of Tf-trHb (A) and Mb (B). The proximal histidine plane (His106) of Tf-trHb is shown to be staggered with respect to the haem nitrogen atoms (A), whereas that of Mb is eclipsed (B). Data from PDB entries 2BMM and 1VXG, respectively.

of the Fe–His stretching modes could, in part, be a consequence of the weakening of the repulsive interactions between the haem and the proximal His, which would allow a stronger Fe coordination.

Moreover, the RR spectra of ferrous WT Tf-trHb share other characteristics with those of other group II bacterial trHbs, such as a haem distortion and the weak intensity of the propionyl bending bands. The haem distortion, revealed by the activation of many out-of-plane modes in the RR low-frequency region, is a consequence of the strain induced on the relatively rigid haem tetrapyrrole ring by the interaction with the protein matrix. Moreover, the weak intensity of the propionyl bending bands is a spectral feature shared by both Tf-trHb and Mt-trHbO, which have an opposite orientation of the haem group with respect to the α,γ-meso axis. It has been shown for Mb, where the haem group is 'reversed', i.e., rotated by 180° around the α,γ-meso axis, that the intensity of the propionyl bending bands is weaker when the haem group has a reversed orientation (Rwere, Mak, & Kincaid, 2008). This finding can be assumed to be a fingerprint of the haem orientation, at least for structurally related proteins.

In conclusion, the RR spectra of the ferrous forms are typical of Class II bacterial Hb and mutations on the distal side of the cavity do not influence the haem distortion or the strength of the proximal His–Fe coordination bond.

5.3 Exogenous Ligands

5.3.1 O_2

At present, although no ν(Fe–O_2) stretching band has been detected by Raman for Tf-trHb, important information on the FeO_2 moiety of Tf-trHb has been obtained by means of MD simulations. After the standard equilibration process to avoid any crash in the starting structure (PDB entry: 2BMM), we performed MD simulations (50 ns) of the Tf-trHb FeO_2 moiety. The results show that two distal site residues (TrpG8 and TyrCD1) interact with the coordinated oxygen molecule (Fig. 6). Both residues act as hydrogen-bond donors to the oxygen molecule, since the coordinated oxygen bears a significant negative charge density due to metal–ligand π-back donation (Marti et al., 2006). The two hydrogen-bond donors provide strong stabilization of the coordinated ligand, which is consistent with a very low dissociation rate constant ($k_{off} = 0.001\ s^{-1}$). These results agree well with those proposed for Mt-tHbO, in which the dioxygen is stabilized by H-bonds provided by the TyrCD1 and the TrpG8 residues, resulting in the extremely slow O_2 off-rate ($0.0014\ s^{-1}$) that is about 10,000-fold slower than for Mb (Ouellet et al., 2003). Moreover, the interplay of

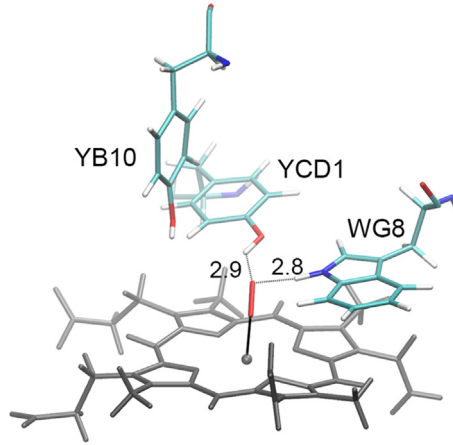

Figure 6 Schematic representation on the basis of MD simulations of a typical snapshot of the distal environment of oxy Tf-trHb showing the H-bonds involving the iron-bound O_2. Distances are in angstroms.

hydrogen-bonding interactions between the haem-bound ligand and the surrounding TyrB10, TrpG8, and HisE7 distal residues in Cj-trHbP has been found to lead to an extremely high oxygen affinity due to a slow dissociation rate (0.0041 s^{-1}) (Arroyo Mañez et al., 2011; Egawa, Wainwright, Poole, & Yeh, 2007).

5.3.2 CO

Two isotope-sensitive peaks (^{12}CO vs. ^{13}CO), assigned to ν(FeC) stretching modes, have been identified in the low-frequency region of the RR spectra of the WT Tf-trHb-CO complex at 509 and 518 cm^{-1}. Accordingly, two ν(CO) stretching modes have been identified at 1940 and 1920 cm^{-1} (Fig. 7). The ν(FeC) and ν(CO) stretching frequencies of WT Tf-trHb and a series of its mutants together with their correlation plot are reported in Fig. 8 and Table 3. The two conformers, identified as form 1 [ν(FeC) and ν(CO) at 509 and 1938 cm^{-1}] and form 2 [ν(FeC) and ν(CO) at 518 and 1920 cm^{-1}], reside in the central and higher parts of the plot, indicating that the bound CO is stabilized by polar interactions. MD simulations have shown that, during the time scale of the simulation, TrpG8 is H-bonded to the coordinated CO. In addition, TyrCD1 is very flexible and can interact with CO, though more weakly than TrpG8 (Fig. 9).

Taken together, these results suggest that the less polar form 1 corresponds to the TrpG8 residue H-bonded to CO, and the more polar form

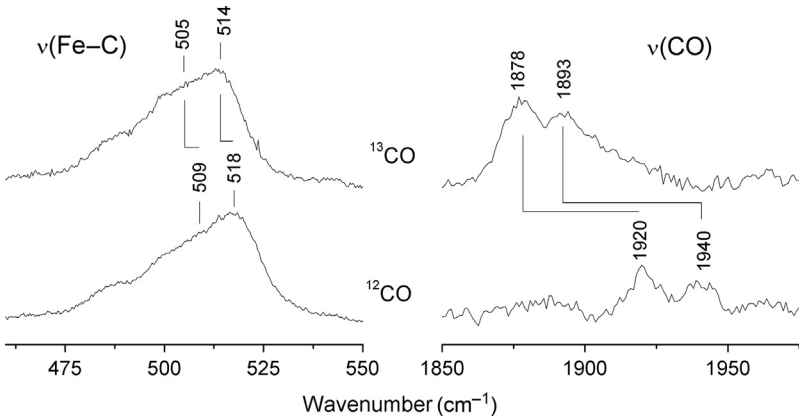

Figure 7 RR spectra of the ^{12}CO and ^{13}CO complexes of WT Tf-trHb. Low-frequency (left) and high-frequency (right) regions showing the ν(Fe–CO) and ν(C–O) stretching modes, respectively.

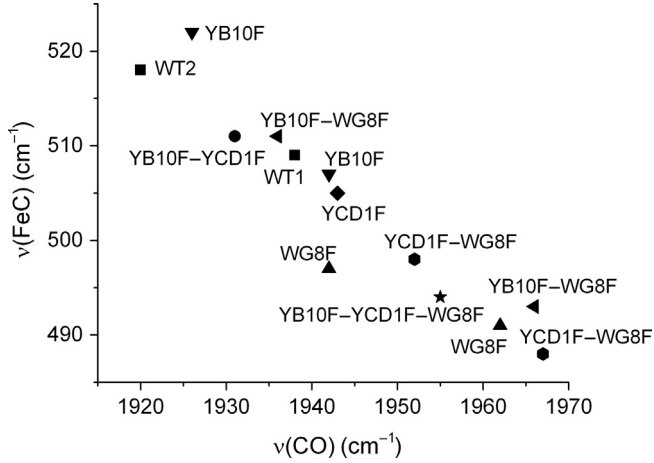

Figure 8 Back-bonding correlation plot for the ν(Fe–C) and ν(C–O) stretching frequencies of WT Tf-trHb and its WG8F, YB10F, YCD1F, YB10F–WG8F, YCD1F–WG8F, YB10F–YCD1F, and YB10F–YCD1F–WG8F mutants. The ν(Fe–C) and ν(C–O) frequencies are reported in Table 3.

2 corresponds to TrpG8 and TyrCD1 that are both H-bonded to the coordinated CO (Fig. 10).

The important role of H-bonding between CO and TrpG8 in the stabilization of both forms 1 and 2 has been highlighted by the spectra of the WG8F mutant (Fig. 11). In fact, for this single mutation the FeCO frequencies are consistent with conformers where polar interactions with the

Table 3 Vibrational Frequencies (cm^{-1}) of the CO Complexes of WT Tf-trHb and Its Mutants (Droghetti et al., 2010)

Proteins	ν(Fe–C) RR	ν(C–O) IR
WT1 (form 1)	509	1938
WT2 (form 2)	518	1920
WG8F	491	1962
	497	1942
YB10F	507	1942
	522	1926
YCD1F	505	1943
YB10F–WG8F	493	1966
	511	1936
YCD1F–WG8F	488	1967
	498	1952
YB10F–YCD1F	511	1931
YB10F–YCD1F–WG8F	494	1955

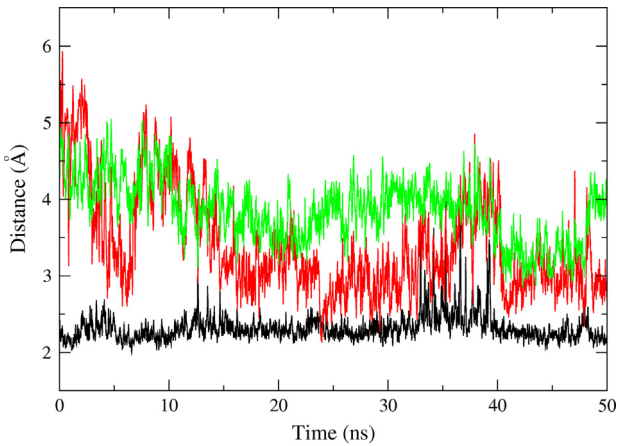

Figure 9 Time evolution of selected hydrogen-bond distances between the H atom of TrpG8Nε (black), the hydroxylic H of TyrCD1 (red (dark grey in the print version)), and the hydroxylic H of TyrB10 (green (grey in the print version)) with the O atom of the coordinated CO. *Adapted with permission from Droghetti et al. (2010). Copyright (2010) American Chemical Society.*

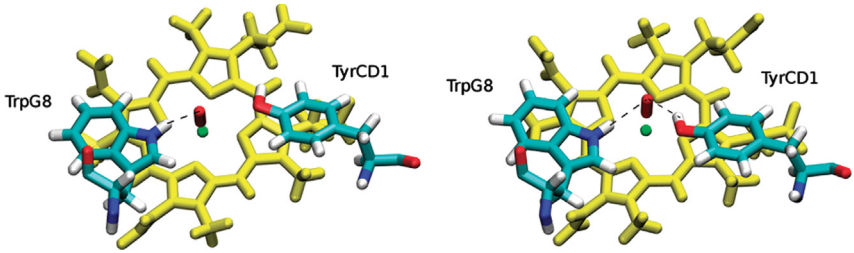

Figure 10 Schematic representation of the distal side of Tf-trHb, showing the H-bonds involving the iron-bound CO in the two forms on the basis of MD simulations. *Adapted with permission from Droghetti et al. (2010). Copyright (2010) American Chemical Society.*

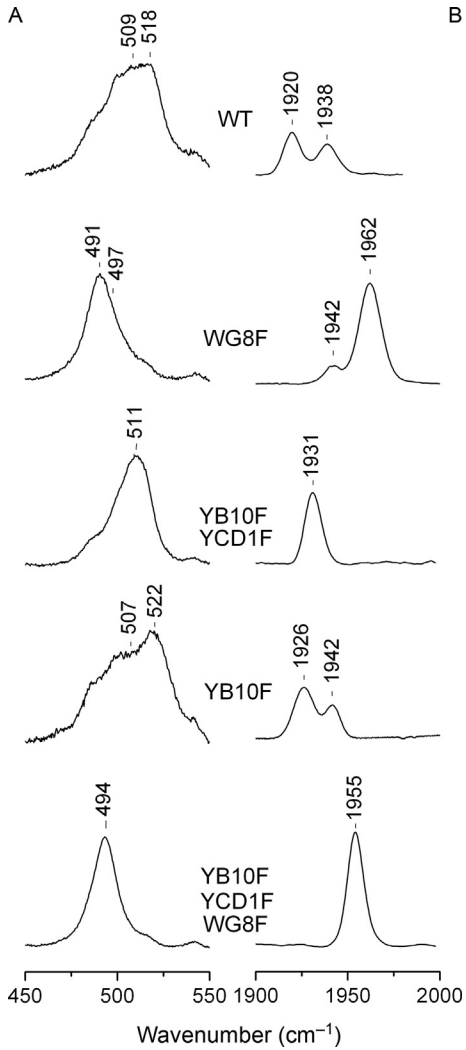

Figure 11 RR (A) and IR (B) spectra of the CO complexes of WT Tf-trHb and selected mutants showing the ν(Fe–CO) and ν(C–O) stretching modes, respectively. *Adapted with permission from Droghetti et al. (2010). Copyright (2010) American Chemical Society.*

surrounding amino acids are absent [ν(FeC) and ν(CO) at 491 and 1962 cm^{-1}, respectively] or weak [ν(FeC) and ν(CO) at 497 and 1942 cm^{-1}, respectively]. Moreover, the spectrum of the double mutant YB10F–YCD1F displays a fairly strong CO-Trp polar interaction [ν(FeC) and ν(CO) at 511 and 1931 cm^{-1}, respectively]. No effect on the characteristics of the CO complex is observed upon mutation of TyrB10 to Phe (YB10F), indicating that this residue is not involved in the stabilization of the CO ligand. Interestingly, as expected, only one apolar form [ν(FeC) at 494 cm^{-1} and ν(CO) at 1955 cm^{-1}] is observed in the case of the triple Phe mutant.

In spite of the similarity of the polar distal cavity with that of Tf-trHb, the CO complex of Mt-trHbO displays only one conformer [ν(FeC) and ν(CO) at 525 and 1914 cm^{-1}, respectively] (see Fig. 2). The mutation of the TyrB10 to Phe does not affect the ν(Fe–CO) frequency; in contrast, the mutation of the TyrCD1 to Phe shifts the ν(Fe–C) frequency to 515 cm^{-1} (Mukai et al., 2002). This suggests that the haem-bound CO in the WT protein is stabilized by an H-bond donated by the phenolic side-chain group of the TyrCD1, but not the TyrB10, which is analogous to the H-bonding network concluded for the hydroxide-bound ferric derivative. The combination of data obtained from RR spectroscopy, mutagenesis, and MD indicates that the haem-bound CO mainly interacts with TrpG8 and TyrCD1 (Guallar, Lu, Borrelli, Egawa, & Yeh, 2009; Ouellet, Milani, et al., 2007; Ouellet, Ranguelova, et al., 2007). These results clearly demonstrate that the distal interactions in Mt-trHbO and Tf-trHb are different, in spite of the occurrence of the Trp–Tyr–Tyr triad in both proteins. The structural difference between the two proteins can possibly be identified with an increased mobility of the distal Tyr residues in Tf-trHb, leading to the appearance of form 1, which is singly H-bonded with TrpG8.

The comparison with Bs-trHbO shows even more striking differences, which can be expected on the basis of the distal cavity structure that is characterized by the polar amino acids TrpG8, TyrB10, and GlnE11 (Feis et al., 2008). The case of the CO complexes of Bs-trHbO can be considered particularly extreme, because the effect of back-bonding on the FeCO vibrational frequencies is one of the strongest observed. In fact, two conformers are observed, the more polar of which displays ν(FeC) and ν(CO) at 545 and 1888 cm^{-1}, respectively (see Fig. 2). Moreover, classical MD simulations show that the CO coordinated to Bs-trHbO interacts strongly with TrpG8 and weakly with GlnE11, which pivots forming and breaking the bond with the coordinated CO (Boechi, Manez, Luque, Marti, & Estrin, 2010).

5.3.3 Fluoride

The fluoride anion binds ferric haem proteins. Although this ligand does not have any physiological role, the combination of RR and UV–vis spectroscopies of fluoride complexes can provide a simple and direct method to monitor the interaction between the distal haem pocket and the iron-bound ligand (Droghetti et al., 2011; Nicoletti, Droghetti, et al., 2011). In fact, as hydrogen bonding is the only effective stabilization mechanism for the haem-bound fluoride, the high sensitivity of fluoride complexes can be used to probe hydrogen bonding in the distal cavity of haem proteins. Recently, the combination of UV–vis, RR, and MD simulations has been applied to study the fluoride complexes of native and distal single, double, and triple mutants of the key WG8, YCD1, and YB10 residues of Tf-trHb (Nicoletti, Droghetti, et al., 2011).

From the comparison of the electronic absorption spectra of the fluoride complexes of WT Tf-trHb, Mb, and HRPC (Fig. 12, left panel, Table 4), it can be seen that unlike the CT2 band maxima (between 451 and 454 nm),

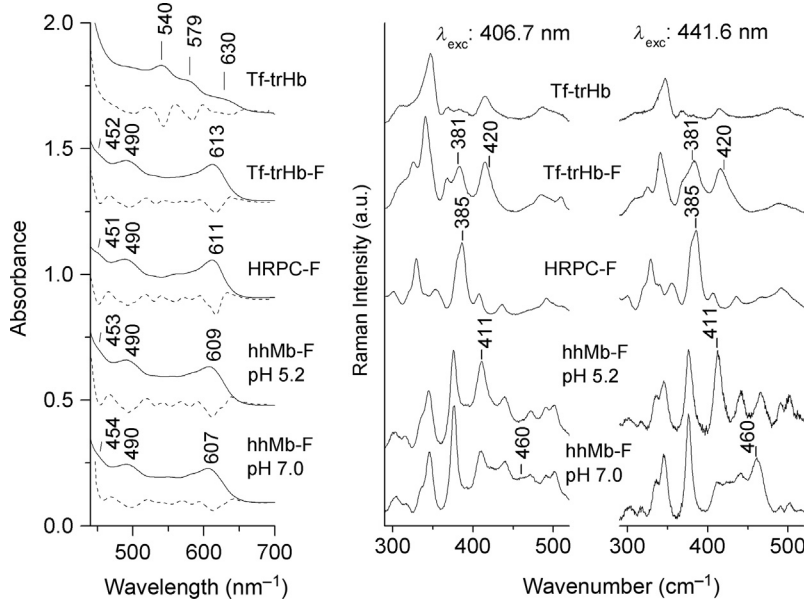

Figure 12 Comparison of the electronic absorption (continuous line), second derivative (dotted line) spectra in the visible region (left), and RR spectra in the low-frequency region taken with excitation in resonance with the Soret (406.7 nm) and with the CT2 band (441.6 nm) (right) of ferric Tf-trHb, together with the fluoride complexes of Tf-trHb, HRPC, and hhMb at pH 7.0 and 5.2. *Adapted from Droghetti et al. (2011). Copyright (2011), with permission from Elsevier.*

Table 4 CT1 Band Maxima (Expressed in nm and cm^{-1}) and ν(Fe–F) Frequencies of WT Tf-trHb and Its Mutants Compared to Those of Mb and HRPC

	CT1 (nm)	CT1 (cm^{-1})	ν(Fe–F) (cm^{-1})	References
YB10F–YCD1F–WG8F	602	16,611	471	Nicoletti, Droghetti, et al. (2011)
YCD1F–WG8F	605	16,529	432	Nicoletti, Droghetti, et al. (2011)
WG8F	609	16,420	421	Nicoletti, Droghetti, et al. (2011)
YCD1F	609	16,420	421	Nicoletti, Droghetti, et al. (2011)
YB10F–YCD1F	609	16,420	419	Nicoletti, Droghetti, et al. (2011)
YB10F–WG8F	610	16,393	415	Nicoletti, Droghetti, et al. (2011)
WT	612	16,340	381 (I) 420 (II)	Nicoletti, Droghetti, et al. (2011)
YB10F	613	16,313	381 (I) 420 (II)	Nicoletti, Droghetti, et al. (2011)
hhMb (pH 7.0)	607	16,474	460	Droghetti et al. (2011)
hhMb (pH 5.2)	609	16,420	411	Droghetti et al. (2011)
HRPC	611	16,367	385	Neri et al. (1997)

which are very similar among the various haem proteins, small but significant differences in the wavelength of the CT1 band are observed. In fact, as expected (Neri et al., 1997), the wavelength of the CT1 band is a sensitive probe of axial ligand polarity and of its interaction with the distal protein residues. In the case of Mb-F complex at neutral pH, the X-ray structure shows that the ligand is doubly H-bonded, with a water molecule and the distal His (Aime et al., 1996). The observed CT1 band occurs at 607 nm, but up-shifts to 609 nm at acidic pH, where a protonated histidine interacts with the ligand. A further up-shift is observed for the HRPC-F complex (CT1 at 611 nm), consistent with the fact that in HRPC the positively charged guanidinium group of the distal Arg together with the distal His stabilizes the anion via H-bonds (Neri et al., 1997). On the basis of these findings, the CT1 maximum at 613 nm observed for Tf-trHb-F is consistent with the presence of multiple H-bonds donated to the fluoride by the distal residues. The RR spectra revealed that Tf-trHb-F is characterized by two conformers with ν(Fe–F) at 420 (conformer 2) and 381 cm^{-1} (conformer 1) (Nicoletti, Droghetti, et al., 2011). This latter is similar to the

spectroscopic signature of haem-containing peroxidases, in agreement with the presence of strong H-bond interactions (Fig. 12, right), while the RR spectrum of horse heart (hh) Mb shows a band at 460 cm^{-1} band at neutral pH which downshifts to 411 cm^{-1} at acid pH (Droghetti et al., 2011).

The presence of multiple strong H-bond interactions in Tf-trHb-F is also demonstrated by the single TrpG8 and TyrCD1 mutants; in the absence of either TrpG8 or TyrCD1, the ν(Fe–F) band shifts to higher frequency, with a concomitant blue-shift of the CT1 band (see Table 4). This observation clearly indicates that the bound fluoride is stabilized by H-bond interactions donated by both TrpG8 and TyrCD1. Conversely, the absence of TyrB10 leads to a strengthening of the H-bond, as observed in the single YB10F mutant and the double YB10F–WG8F and YB10–YCD1 mutants. Based on the Raman measurements, we concluded that in the presence of TrpG8 and TyrCD1, TyrB10 does not interact with the ligand. In fact, TyrB10 is able to weakly interact with fluoride only when H-bond interactions with both TrpG8 and TyrCD1 are missing (Nicoletti, Droghetti, et al., 2011).

As observed for the case of the oxygen ligand and in agreement with the RR results, MD simulations of the fluoride adducts of the WT protein show that two distal site residues interact with the coordinated ligand: TrpG8 and TyrCD1 act as hydrogen-bond donors for the polar coordinated fluoride (Nicoletti, Droghetti, et al., 2011). However, an MD simulation (50 ns) performed recently shows that TyrB10 can interact weakly with the fluoride via a water molecule in one of the protein conformations (conformer 1), while no interaction is present in conformer 2 (Fig. 13A and B). The MD simulations of the single and double mutants well agree with the RR results (Fig. 13C–H), showing that when TrpG8 and/or TyrCD1 are absent, TyrB10 interacts with the fluoride and the interaction depends on the presence of water molecules that occupy the distal site dynamically (Fig. 13C, E, and F).

A linear correlation has been found between the frequencies of the ν(Fe–F) stretching mode and the CT1 band for the Tf-trHb fluoride complexes of the WT and mutant proteins. The validity of the correlation has been confirmed by its application to the literature data of Mb, HRPC, and DHP (Nicoletti, Droghetti, et al., 2011). As can be seen from Fig. 14, the spectroscopic markers of the fluoride complexes [ν(Fe–F) and CT1 wavenumbers] are fitted well by a straight line with positive slope. The (CT1)/ν(Fe–F) position along the correlation line reflects the extent of distal H-bonding interactions. Fluoride complexes in which the ligand is stabilized by multiple, strong H-bond interactions, like those of the WT Tf-trHb and

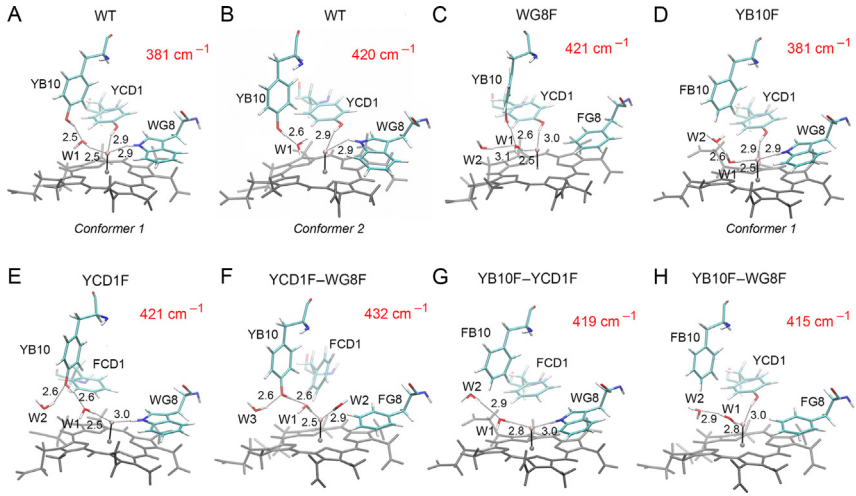

Figure 13 Schematic representation of the distal haem cavity of the mutated proteins with fluoride showing, on the basis of MD simulations, the hydrogen-bond network (dotted lines) stabilizing the fluoride for WT (A and B), single (C–E), and double (F–H) mutant proteins. TyrB10, WG8, and YCD1 are H-bond donors. Distances are in angstroms. The RR ν(Fe–F) stretching frequencies for each mutant are shown in red. For the YB10F mutant, only conformer 1 is shown.

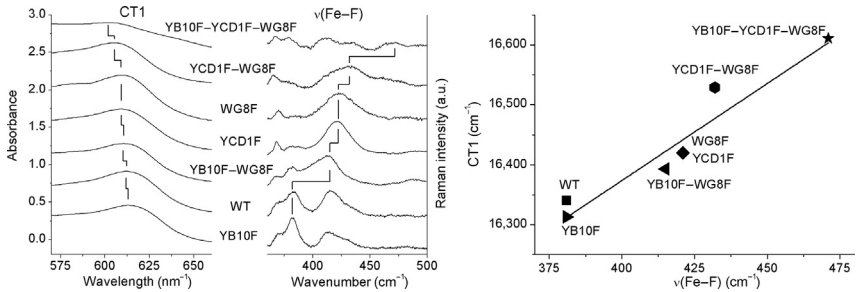

Figure 14 (Left) Variation of the CT1 wavelength and corresponding ν(Fe–F) wavenumbers of the fluoride adducts of WT Tf-trHb and its mutants YB10F, YCD1F, WG8F, YB10F–WG8F, YCD1F–WG8F, and YB10F–YCD1F–WG8F. (Right) Empirical correlation plot between the ν(Fe–F) wavenumbers and the CT1 energy of WT Tf-trHb and its mutants. The experimental data are reported in Table 4. The line represents a least-squares fit of the experimental data of WT Tf-trHb and the combinatorial set of its mutants considering only the strongly H-bonded forms of WT and YB10F with the ν(Fe–F) stretch at 381 cm^{-1}.

YB10F conformer that is characterized by a ν(Fe–F) frequency at 381 cm^{-1}, are located at the extreme left side. In fact, H-bonding decreases both the ν(Fe–F) stretching frequency and the energy of the $e_g(d\pi)$ orbitals, thereby lowering the energy of the $a_{2u}(\pi) \rightarrow e_g(d\pi)$ CT1 transition. At the other extremity of the line, fluoride complexes with very weak H-bond interactions are found, like that of the triple mutant (YB10F–YCD1F–WG8F). In the central region, the complexes characterized by one or two H-bonds can be found.

5.3.4 H_2S

The first observation of a high-affinity sulphide-binding Hb concerned haemoglobin I (HbI) from the mollusc *L. pectinata*, which binds sulphide in its ferric state and functions as a sulphide carrier (Kraus & Wittenberg, 1990). Recently, Bs-trHbO and Tf-trHbO (Fig. 15) were found to bind sulphide (Nicoletti et al., 2010). The electronic absorption and RR data indicate that the sulphide adducts are typical of a ferric iron LS derivative characterized, in analogy with other LS ferric sulphide adducts, by the strong Fe–S stretching band at 375 cm^{-1}.

Both proteins possess a high affinity for hydrogen sulphide at pH 7.0, though lower than that reported previously for *L. pectinata* HbI (Kraus & Wittenberg, 1990) (Table 5). The high sulphide affinity of these proteins must have a physiological significance as H_2S is produced in bacteria at metabolic steps involved in cysteine biosynthesis and, hence, in thiol redox homeostasis. Thiol-based switches have recently been demonstrated to be common in protein sensors of antioxidant cascades, in both prokaryotic and eukaryotic organisms. Several redox sensors, under the master control of OxyR, respond to hydrogen peroxide stress by formation of disulphide bonds. TrHbs have been shown to be part of an operon linked to OxyR, at least in Bacillus species (Larsson, Rogstam, & von Wachenfeldt, 2007). In this framework, a role of microbial globins in modulating H_2S signalling and/or thiol oxidation (the so-called disulphide stress) has been proposed (Nicoletti et al., 2010).

From a kinetic point of view, the overall high affinity resides in the slow rate of sulphide release, attributed to hydrogen-bonding stabilization of the bound ligand by the distal WG8 residue. A set of point mutants in which distal residues have been replaced with Phe indicates that the WG8 residue represents the major kinetic barrier to the escape of the bound sulphide species. Accordingly, classical MD simulations of Tf-trHbO with coordinated HS^- indicate that WG8 plays a key role in the stabilization of coordinated

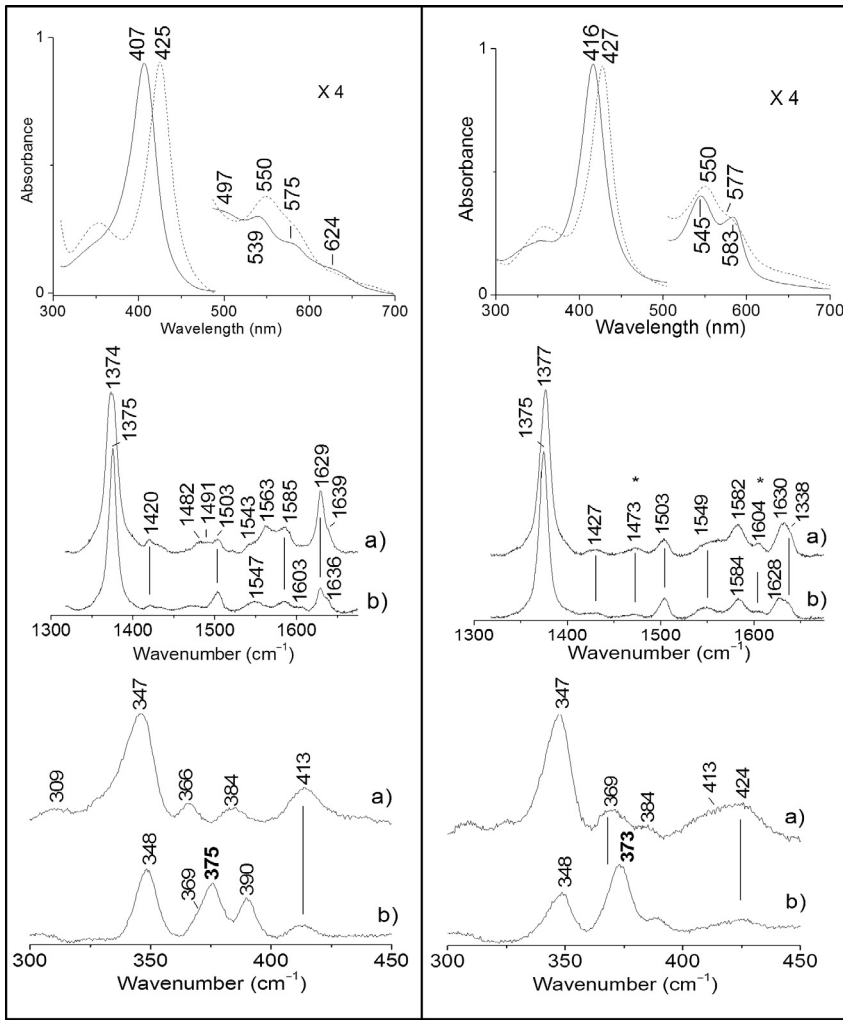

Figure 15 Comparison of the electronic absorption and resonance Raman spectra of WT ferric *T. fusca* (left) and *B. subtilis* (right), in the absence (—, a) and presence of Na_2S (---, b). (Top) Absorption spectra, (middle) high-frequency, and (bottom) low-frequency RR spectra. The ν(Fe–S) is indicated in bold. The asterisk indicates spurious bands of the deoxy form deriving from the photolysis of the ferrous-oxy species present in Bs-trHb in small quantities. *Adapted with permission from Nicoletti et al. (2010). Copyright (2010) American Chemical Society.*

SH^-, whereas the YCD1 and YB10 contributions are negligible (Fig. 16). Interestingly, when TrpG8 is mutated to a hydrophobic residue, such as Phe (both in the single mutant WG8F and in the triple mutant WG8F–YB10F–YCD1F), the dissociation constant increases by about two orders of

Table 5 Thermodynamic and Kinetic Constants for Sulphide Binding to Various Haem Proteins (Nicoletti et al., 2010)

Protein	$K_{(HS^-)}(M^{-1})$	$k_{(HS^-)}(M^{-1}s^{-1})$	$k'_{(HS^-)}(s^{-1})$	References
Bs-trHb	5.0×10^6	1.3×10^4	0.0026	Nicoletti et al. (2010)
Tf-trHb	2.8×10^6	5×10^3	0.0018	Nicoletti et al. (2010)
WG8F–YB10F–YCD1F *Tf-trHb*	2.0×10^7	4.4×10^6	0.22	Nicoletti et al. (2010)
swMb	5×10^4			Jorgensen, Chandrasekar, Madura, Impey, and Klein (1983)
L29F–H64Q–V68F swMb	3.7×10^7			Jorgensen et al. (1983)
L. pectinata HbI	1.1×10^7	2.3×10^5	0.00022	Kraus and Wittenberg (1990)
L. pectinata HbII	1.7×10^4	1.13×10^4	0.017	Kraus and Wittenberg (1990)
L. pectinata HbIII	2.5×10^4	$1–4 \times 10^4$	0.016	Kraus and Wittenberg (1990)

magnitude, implying a weakened stabilization of the iron-bound sulphide (Table 5). This is in agreement with the notion that hydrogen bonding is the main kinetic control of ligand dissociation in haem proteins and confirms the role of TrpG8 in sulphide stabilization in trHbs.

6. CONCLUDING REMARKS

The body of experimental observations and MD simulations here reviewed indicates that a multiplicity of interactions modulate the properties of Fe–ligand moieties in trHbs and, hence, dominate the dynamics of ligand entry and escape and possibly also modulate ligand stabilization. The subtle features of each Fe–ligand complex must be considered in order to account for the observed differences in ligand-binding behaviour. For example, both the experimental and MD simulations data indicate that, as in the case of the CO adducts (Droghetti et al., 2010), TrpG8 and TyrCD1 can form strong hydrogen bonds with fluoride, whereas TyrB10 plays only a minor role in

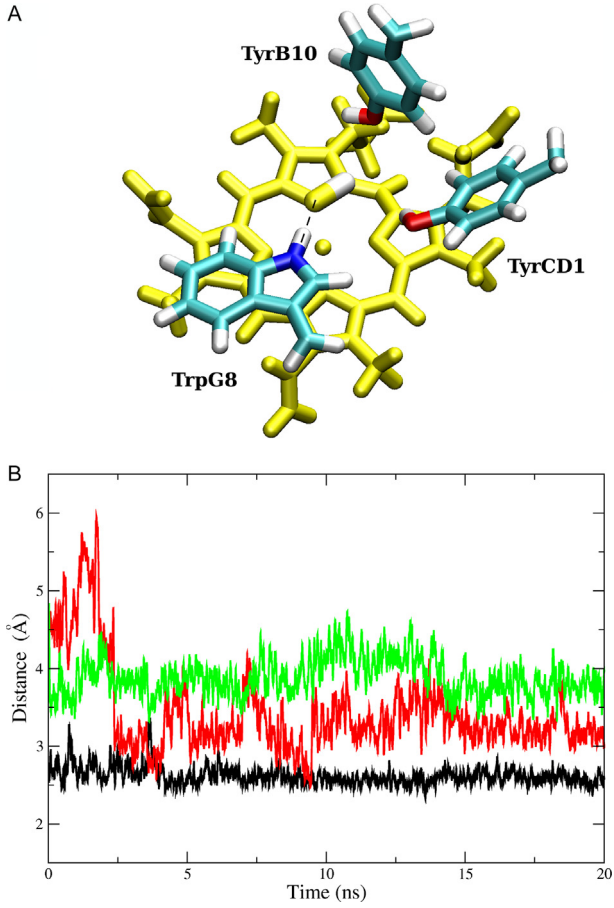

Figure 16 (A) Schematic representation of the WT Tf-trHb distal site with coordinated SH^-, showing the residues of the distal site (TrpG8, TyrCD1, and TyrB10). (B) Time evolution of selected distances among distal residues and haem-bound SH^- of WT Tf-trHb. The distances correspond to those between the S-atom of the coordinated SH^- and the indole N proton of TrpG8 (black), the hydroxyl hydrogen of TyrCD1 (red (dark grey in the print version)), and the hydroxyl hydrogen of TyrB10 (green (grey in the print version)). *Adapted with permission from Nicoletti et al. (2010). Copyright (2010) American Chemical Society.*

the stabilization of the ligand. However, when the effects of the mutations on the RR spectra are compared, the corresponding complexes exhibit different behaviour, since back-bonding in the CO complexes depends on many kinds of polar interactions with the neighbouring amino acids, while hydrogen bonding is the only effective stabilization mechanism for the haem-bound fluoride. Moreover, the two types of complex have different

chemical properties since carbon monoxide bears less charge density than fluoride. On the other hand, the HS^- ligand establishes strong H-bonding interactions between the S-atom of the coordinated sulphide, which bears a significant negative charge density, and H-bond donating amino acids. In turn, molecular oxygen offers the possibility of concomitant interactions with all three main H-bond donors. As a consequence, iron-bound oxygen remains confined within the H-bonding network with little possibility to escape from within the haem pocket.

Taken together, these results highlight the considerable potential afforded by the combination of RR spectroscopy and the microscopic complementary insight provided by MD simulations to widen our understanding on the complex interactions that modulate the relationship between structure and reactivity in this important group of proteins.

ACKNOWLEDGEMENTS

We thank members of our research groups and co-workers who are responsible for some of the work reviewed in this chapter; their names are listed in the appropriate references. We would particularly like to thank for their contribution Dr. Alessandra Bonamore, Mr. Juan P. Bustamante, Dr. Enrica Droghetti, Dr. Alessandro Feis, and Dr. Francesco P. Nicoletti.

REFERENCES

Adar, F. (1978). Electronic absorption spectra of hemes and hemoproteins. In D. Dolphin (Ed.), *Physical chemistry, part A: Vol. 3. The porphyrins* (pp. 167–209). New York: Academic Press.

Aime, S., Fasano, M., Paoletti, S., Cutruzzola, F., Desideri, A., Bolognesi, M., et al. (1996). Structural determinants of fluoride and formate binding to hemoglobin and myoglobin: Crystallographic and 1H-NMR relaxometric study. *Biophysical Journal*, *70*, 482–488.

Arroyo Mañez, P., Lu, C., Boechi, L., Marti, M. A., Shepherd, M., Wilson, J. L., et al. (2011). Role of the distal hydrogen-bonding network in regulating oxygen affinity in the truncated hemoglobin III from *Campylobacter jejuni*. *Biochemistry*, *50*, 3946–3956.

Arya, S., Sethi, D., Singh, S., Hade, M. D., Singh, V., Raju, P., et al. (2013). Truncated hemoglobin, HbN, is post-translationally modified in *Mycobacterium tuberculosis* and modulates host-pathogen interactions during intracellular infection. *The Journal of Biological Chemistry*, *288*, 29987–29999.

Bailly, X., & Vinogradov, S. (2005). The sulfide binding function of annelid hemoglobins: Relic of an old biosystem? *Journal of Inorganic Biochemistry*, *99*, 142–150.

Bidon-Chanal, A., Martí, M. A., Crespo, A., Milani, M., Orozco, M., Luque, F. J., et al. (2006). Ligand-induced dynamical regulation of NO conversion in *Mycobacterium tuberculosis* truncated hemoglobin-N. *Proteins*, *64*, 457–464.

Bieza, S. A., Boubeta, F., Feis, A., Smulevich, G., Estrin, D. A., Boechi, L., et al. (2015). Reactivity of inorganic sulfide species toward a heme protein model. *Inorganic Chemistry*, *54*, 527–533.

Boechi, L., Manez, P. A., Luque, F. J., Marti, M. A., & Estrin, D. A. (2010). Unraveling the molecular basis for ligand binding in truncated hemoglobins: The trHbO *Bacillus subtilis* case. *Proteins*, *78*, 962–970.

Boechi, L., Martí, M. A., Milani, M., Bolognesi, M., Luque, F. J., & Estrin, D. A. (2008). Structural determinants of ligand migration in *Mycobacterium tuberculosis* truncated hemoglobin O. *Proteins*, *73*, 372–379.

Boffi, A., Rizzi, M., Monacelli, F., & Ascenzi, P. (2000). Determination of H2S solubility via the reaction with ferric hemoglobin I from the bivalve mollusc *Lucina pectinata*. *Biochimica et Biophysica Acta*, *1523*, 206–208.

Bonamore, A., Ilari, A., Giangiacomo, L., Bellelli, A., Morea, V., & Boffi, A. (2005). A novel thermostable hemoglobin from the actinobacterium *Thermobifida fusca*. *FEBS Journal*, *272*, 4189–4201.

Brunner, H. (1974). Identification of the iron-ligand vibration of oxyhemoglobin. *Naturwissenschaften*, *61*, 129.

Capece, L., Boechi, L., Perissinotti, L. L., Arroyo-Mañez, P., Bikiel, D. E., Smulevich, G., et al. (2013). Small ligand-globin interactions: Reviewing lessons derived from computer simulation. *Biochimica et Biophysica Acta*, *1834*, 1722–1738.

Cerda, J., Echevarria, Y., Morales, E., & Lopez-Garriga, J. (1999). Resonance Raman studies of the heme-ligand active site of haemoglobin I from *Lucina pectinata*. *Biospectroscopy*, *5*, 289–301.

Choi, S., Spiro, T. G., Langry, K. C., Smith, K. M., Budd, D. L., & La Mar, G. N. (1982). Structural correlations and vinyl influences in resonance Raman spectra of protoheme complexes and proteins. *Journal of the American Chemical Society*, *104*, 4345–4351.

Couture, M., Yeh, S.-R., Wittenberg, B. A., Wittenberg, J. B., Ouellet, Y., Rousseau, D. L., et al. (1999). A cooperative oxygen-binding hemoglobin from *Mycobacterium tuberculosis*. *Proceedings of the National Academy of Sciences of the United States of America*, *96*, 11223–11228.

Das, T. K., Couture, M., Ouellet, Y., Guertin, M., & Rousseau, D. L. (2001). Simultaneous observation of the O—O and Fe—O_2 stretching modes in oxyhemoglobins. *Proceedings of the National Academy of Sciences of the United States of America*, *98*, 479–484.

Desbois, A., Lutz, M., & Banerjee, R. (1979). Low-frequency vibrations in resonance Raman spectra of horse heart myoglobin. Iron-ligand and iron-nitrogen vibrational modes. *Biochemistry*, *18*, 1510–1518.

Droghetti, E., Nicoletti, F. P., Bonamore, A., Boechi, L., Arroyo-Mañez, P., Estrin, D. A., et al. (2010). Hemepocket structural properties of a bacterial truncated hemoglobin from *Thermobifida fusca*. *Biochemistry*, *49*, 10394–10402.

Droghetti, E., Nicoletti, F. P., Bonamore, A., Sciamanna, N., Boffi, A., Feis, A., et al. (2011). The optical spectra of fluoride complexes can effectively probe H-bonding interactions in the distal cavity of heme proteins. *Journal of Inorganic Biochemistry*, *105*, 1338–1343.

Duff, L. L., Appelman, E. H., Shriver, D. F., & Klots, I. M. (1979). Steric disposition of O_2 in oxyhemoglobin as revealed by its resonance Raman spectrum. *Biochemical and Biophysical Research Communications*, *90*, 1098–1103.

Edwards, S. L., & Poulos, T. L. (1990). Ligand binding and structural perturbations in cytochrome c peroxidase. *The Journal of Biological Chemistry*, *265*, 2588–2595.

Egawa, T., Wainwright, L. M., Poole, R. K., & Yeh, S.-R. (2007). Structural and functional properties of a truncated hemoglobin from a food-borne pathogen *Campylobacter jejuni*. *The Journal of Biological Chemistry*, *282*, 13627–13636.

Egawa, T., & Yeh, S.-R. (2005). Structural and functional properties of hemoglobins from unicellular organisms as revealed by resonance Raman spectroscopy. *Journal of Inorganic Biochemistry*, *99*, 72–96.

Elber, R. (2010). Ligand diffusion in globins: Simulations versus experiment. *Current Opinion in Structural Biology*, *20*, 162–167.

Evangelista-Kirkup, R., Smulevich, G., & Spiro, T. G. (1986). Alternative carbon monoxide binding modes for horseradish peroxidase studied by resonance Raman spectroscopy. *Biochemistry*, *25*, 4420–4425.

Feis, A., Lapini, A., Catacchio, B., Brogioni, S., Foggi, P., Chiancone, E., et al. (2008). Unusually strong H-bonding to the heme ligand and fast geminate recombination dynamics of the carbon monoxide complex of *Bacillus subtilis* truncated hemoglobin. *Biochemistry*, *47*, 902–910.

Feis, A., Marzocchi, M. P., & Smulevich, G. (1994). Spin-state and axial ligand bonding in the hydroxy complexes of metmyoglobin, methemoglobin, and horseradish peroxidase at room and low temperatures. *Biochemistry*, *33*, 4577–4583.

Feis, A., Rodriguez-Lopez, J. N., Thorneley, R. N. F., & Smulevich, G. (1998). The distal cavity structure of carbonyl horseradish peroxidase as probed by the resonance Raman spectra of His42Leu and Arg38Leu mutants. *Biochemistry*, *37*, 13575–13581.

Forti, F., Boechi, L., Bikiel, D., Martí, M. A., Nardini, M., Bolognesi, M., et al. (2011). Ligand migration in *Methanosarcina acetivorans* protoglobin: Effects of ligand binding and dimeric assembly. *The Journal of Physical Chemistry B*, *115*, 13771–13780.

Freitas, T. A., Hou, S., Dioum, E. M., Saito, J. A., Newhouse, J., Gonzalez, G., et al. (2004). Ancestral hemoglobins in Archaea. *Proceedings of the National Academy of Sciences of the United States of America*, *101*, 6675–6680.

Frey, A. D., & Kallio, P. T. (2003). Bacterial hemoglobins and flavohemoglobins: Versatile proteins and their impact on microbiology and biotechnology. *FEMS Microbiology Reviews*, *27*, 525–545.

Giangiacomo, L., Ilari, A., Boffi, A., Morea, V., & Chiancone, E. (2005). The truncated oxygen-avid hemoglobin from *Bacillus subtilis:* X-ray structure and ligand binding properties. *The Journal of Biological Chemistry*, *280*, 192–202.

Giordano, D., Pesce, A., Boechi, L., Bustamante, J. P., Caldelli, E., Howes, B. D., et al. (2015). Structural flexibility of the heme cavity in the cold-adapted truncated hemoglobin from the Antarctic marine bacterium *Pseudoalteromonas haloplanktis* TAC125. *The FEBS Journal*, *282*, 2948–2965.

Giordano, D., Russo, R., Ciaccio, C., Howes, B. D., di Prisco, G., Marden, M. C., et al. (2011). Ligand- and proton-linked conformational changes of the ferrous 2/2 hemoglobin of *Pseudoalteromonas haloplanktis* TAC125. *IUBMB Life*, *63*, 566–573.

Gouterman, M. (1978). Optical spectra and electronic structure of porphyrins and related rings. In D. Dolphin (Ed.), *The porphyrins: Vol. 3*. (pp. 1–165). New York: Academic Press.

Guallar, V., Lu, C., Borrelli, K., Egawa, T., & Yeh, S. R. (2009). Ligand migration in the truncated hemoglobin-II from *Mycobacterium tuberculosis*: The role of G8 tryptophan. *The Journal of Biological Chemistry*, *284*, 3106–3116.

Guallar, V., & Wallrapp, F. H. (2011). QM/MM methods: Looking inside heme proteins biochemistry. *Biophysical Chemistry*, *149*, 1–11.

Hill, B. C., & Nicholls, P. (1980). Cytochrome c reduction by cysteine plus copper: A pseudo substrate system for cytochrome c oxidase. *Canadian Journal of Biochemistry*, *58*, 499–503.

Hirota, S., Li, T., Phillips, G. N., Jr., Olson, J. S., Mukai, M., & Kitagawa, T. (1996). Perturbation of the Fe-O_2 bond by nearby residues in heme pocket: Observation of Fe-O_2 Raman bands for oxymyoglobin mutants. *Journal of the American Chemical Society*, *118*, 7845–7846.

Hori, H., & Kitagawa, T. (1980). Iron-ligand stretching band in the resonance Raman spectra of ferrous iron porphyrin derivatives. Importance as a probe band for quaternary structure of hemoglobin. *Journal of the American Chemical Society*, *102*, 3608–3613.

Howes, B. D., Feis, A., Indiani, C., Marzocchi, M. P., & Smulevich, G. (2000). Formation of two types of low-spin heme in horseradish peroxidase isoenzyme A2 at low temperature. *Journal of Biological Inorganic Chemistry*, *5*, 227–235.

Howes, B. D., Helbo, S., Fago, A., & Smulevich, G. (2012). Insights into the anomalous heme pocket of rainbow trout myoglobin. *Journal of Inorganic Biochemistry*, *109*, 1–8.

Howes, B. D., Rodriguez-Lopez, J. N., Smith, A. T., & Smulevich, G. (1997). Mutation of distal residues of horseradish peroxidase: Influence on substrate binding and cavity properties. *Biochemistry*, *36*, 1532–1543.

Jensen, F. B. (2009). The dual roles of red blood cells in tissue oxygen delivery: Oxygen carriers and regulators of local blood flow. *Journal of Experimental Biology*, *212*, 3387–3393.

Jorgensen, W. L., Chandrasekar, J., Madura, J., Impey, R. W., & Klein, M. L. (1983). Comparison of simple potential functions for simulating liquid water. *Journal of Chemical Physics*, *79*, 926–935.

Karplus, M. L., & McCammon, J. A. (2002). Molecular dynamics simulations of biomolecules. *Nature Structural Biology*, *9*, 646–652.

Keilin, D. (1933). On the combination of methaemoglobin with H2S. *Proceedings of the Royal Society B*, *133*, 393–404.

Keilin, D. (1953). Haemoglobin in fungi. Occurrence of haemoglobin in yeast and the supposed stabilization of the oxygenated cytochrome oxidase. *Nature*, *172*, 390–393.

Kerr, E. A., & Yu, N.-T. (1988). Vibrational modes of coordinated CO, CN^- and NO. In T. G. Spiro (Ed.), *Biological applications of Raman spectroscopy: Vol. 3.* (pp. 39–95). New York: John Wiley and Sons, Inc.

Kitagawa, T. (1988). The heme protein structure and the iron histidine stretching mode. In T. G. Spiro (Ed.), *Biological applications of Raman spectroscopy: Resonance Raman spectra of hemes and metalloproteins: Vol. 3.* (pp. 97–131). New York: Wiley.

Kitagawa, T., Nagai, K., & Tsubaki, M. (1979). Assignment of the Fe-N epsilon (His F8) stretching band in the resonance Raman spectra of deoxy myoglobin. *FEBS Letters*, *104*, 376–378.

Kraus, D. W., & Wittenberg, J. B. (1990). Hemoglobins of the *Lucina pectinata*/bacteria symbiosis. I. Molecular properties, kinetics and equilibria of reactions with ligands. *The Journal of Biological Chemistry*, *265*, 16043–16053.

Larsson, J. T., Rogstam, A., & von Wachenfeldt, C. (2007). YjbH is a novel negative effector of the disulphide stress regulator, Spx, in Bacillus subtilis. *Molecular Microbiology*, *66*, 669–684.

Li, T. S., Quillin, M. L., Philips, G. N., & Olson, J. S. (1994). Structural determinants of the stretching frequency of CO bound to myoglobin. *Biochemistry*, *33*, 1433–1446.

Ling, J. H., Li, T. S., Olson, J. S., & Bocian, D. F. (1994). Identification of the iron-carbonyl stretch in distal histidine mutants of carbonmonoxymyoglobin. *Biochimica et Biophysica Acta, Bioenergetics*, *1188*, 417–421.

Lu, C., Egawa, T., Mukai, M., Poole, R. K., & Yeh, S.-R. (2008). Hemoglobins from *Mycobacterium tuberculosis* and *Campylobacter jejuni*: A comparative study with resonance Raman spectroscopy. In R. K. Poole (Ed.), *Methods in enzymology: Vol. 437.* (pp. 256–286). New York: Elsevier.

Lu, C., Egawa, T., Wainwright, L. M., Poole, R. K., & Yeh, S. R. (2007). Structural and functional properties of a truncated hemoglobin from a food-borne pathogen *Campylobacter jejuni*. *The Journal of Biological Chemistry*, *282*, 13627–13636.

Marti, M. A., Crespo, A., Capece, L., Boechi, L., Bikiel, D. E., Scherlis, D. A., et al. (2006). Dioxygen affinity in heme proteins investigated by computer simulation. *Journal of Inorganic Biochemistry*, *100*, 761–770.

Martínková, M., Kitanishi, K., & Shimizu, T. (2013). Heme-based globin-coupled oxygen sensors: Linking oxygen binding to functional regulation of diguanylate cyclase, histidine kinase, and methyl-accepting chemotaxis. *The Journal of Biological Chemistry*, *288*, 27702–27711.

Milani, M., Savard, P. Y., Ouellet, H., Ascenzi, P., Guertin, M., & Bolognesi, M. (2003). A TyrCD1/TrpG8 hydrogen bond network and a TyrB10-TyrCD1 covalent link shape the heme distal site of *Mycobacterium tuberculosis* hemoglobin O. *Proceedings of the National Academy of Sciences of the United States of America*, *100*, 5766–5771.

Mukai, M., Savard, P. Y., Ouellet, H., Guertin, M., & Yeh, S.-R. (2002). Unique ligand protein interactions in a new truncated hemoglobin from *Mycobacterium tuberculosis*. *Biochemistry*, *41*, 3897–3905.

Nagai, K., Kitagawa, T., & Morimoto, H. (1980). Quaternary structures and low frequency molecular vibrations of haems of deoxy and oxyhaemoglobin studied by resonance Raman scattering. *Journal of Molecular Biology*, *136*, 271–289.

Neri, F., Kok, D., Miller, M. A., & Smulevich, G. (1997). Fluoride binding in hemoproteins: The importance of the distal cavity structure. *Biochemistry*, *36*, 8947–8953.

Nicholls, P. (1961). The formation and properties of sulphmyoglobin and sulphcatalase. *Biochemical Journal*, *81*, 374–383.

Nicoletti, F. P., Bustamante, J. P., Droghetti, E., Howes, B. D., Fittipaldi, M., Bonamore, A., et al. (2014). Interplay of the H-bond donor-acceptor role of the distal residues in hydroxyl ligand stabilization of *Thermobifida fusca* truncated hemoglobin. *Biochemistry*, *53*, 8021–8030.

Nicoletti, F. P., Comandini, A., Bonamore, A., Boechi, L., Boubeta, F. M., Feis, A., et al. (2010). Sulfide binding properties of truncated hemoglobins. *Biochemistry*, *49*, 2269–2278.

Nicoletti, F. P., Droghetti, E., Boechi, L., Bonamore, A., Sciamanna, N., Estrin, D. A., et al. (2011). Fluoride as a probe for H-bonding interactions in the active site of heme proteins: The case of *Thermobifida fusca* hemoglobin. *Journal of the American Chemical Society*, *133*, 20970–20980.

Nicoletti, F. P., Droghetti, E., Howes, B. D., Bustamante, J. P., Bonamore, A., Sciamanna, N., et al. (2013). H-bonding networks of the distal residues and water molecules in the active site of *Thermobifida fusca* hemoglobin. *Biochimica et Biophysica Acta*, *1834*, 1901–1909.

Nicoletti, F. P., Thompson, M. K., Franzen, S., & Smulevich, G. (2011). Degradation of sulfide by dehaloperoxidase-hemoglobin from *Amphitrite ornata*. *Journal of Biological Inorganic Chemistry*, *16*, 611–619.

Nissum, M., Feis, A., & Smulevich, G. (1998). Characterization of soybean seed coat peroxidase: Resonance Raman evidence for a structure based classification of plant peroxidases. *Biospectroscopy*, *4*, 355–364.

Norberg, J. L., & Nilsson, L. (2002). Molecular dynamics applied to nucleic acids. *Accounts of Chemical Research*, *35*, 465–472.

Ouellet, H., Juszczak, L., Dantsker, D., Samuni, U., Ouellet, Y. H., Savard, P. Y., et al. (2003). Reactions of *Mycobacterium tuberculosis* truncated hemoglobin O with ligands reveal a novel ligand-inclusive hydrogen bond network. *Biochemistry*, *42*, 5764–5774.

Ouellet, H., Milani, M., LaBarre, M., Bolognesi, M., Couture, M., & Guertin, M. (2007). The roles of Tyr(CD1) and Trp(G8) in *Mycobacterium tuberculosis* truncated hemoglobin O in ligand binding and on the heme distal site architecture. *Biochemistry*, *46*, 11440–11450.

Ouellet, H., Ranguelova, K., Labarre, M., Wittenberg, J. B., Wittenberg, B. A., Magliozzo, R. S., et al. (2007). Reaction of Mycobacterium tuberculosis truncated hemoglobin O with hydrogen peroxide: Evidence for peroxidatic activity and formation of protein-based radicals. *The Journal of Biological Chemistry*, *282*, 7491–7503.

Pesce, A., Bolognesi, M., & Nardini, M. (2013). The diversity of 2/2 (truncated) globins. *Advances in Microbial Physiology*, *63*, 49–78.

Phillips, G. N., Jr., Teodoro, M. L., Li, T., Smith, B., & Olson, J. S. (1999). Bound CO is a molecular probe of electrostatic potential in the distal pocket of myoglobin. *The Journal of Physical Chemistry B*, *103*, 8817–8829.

Pietri, R., Lewis, A., Leon, R. G., Casabona, G., Kiger, L., Yeh, S. R., et al. (2009). Factors controlling the reactivity of hydrogen sulfide with hemeproteins. *Biochemistry*, *48*, 4881–4894.

Pietri, R., Roman-Morales, E., & Lopez-Garriga, J. (2011). Hydrogen sulfide and hemeproteins: Knowledge and mysteries. *Antioxidants and Redox Signaling*, *15*, 393–404.

Ríos-Gonzalez, B. B., Roman-Morales, E. M., Pietri, R., & Lopez-Garriga, J. (2014). Hydrogen sulfide activation in hemeproteins: The sulfheme scenario. *Journal of Inorganic Biochemistry*, *133*, 78–86.

Rodriguez, J. C., Zeng, Y., Wilks, A., & Rivera, M. (2007). The hydrogen-bonding network in heme oxygenase also functions as a modulator of enzyme dynamics: Chaotic motions upon disrupting the H-bond network in heme oxygenase from *Pseudomonas aeruginosa*. *Journal of the American Chemical Society*, *129*, 11730–11742.

Roux, B., & Schulten, K. (2004). Computational studies of membrane channels. *Structure*, *12*, 1343–1351.

Rwere, F., Mak, P. J., & Kincaid, J. R. (2008). Resonance Raman interrogation of the consequences of heme rotational disorder in myoglobin and its ligated derivatives. *Biochemistry*, *47*, 12869–12877.

Samuni, U., Ouellet, Y., Guertin, M., Friedman, J. M., & Yeh, S. R. (2004). The absence of proximal strain in the truncated hemoglobins from *Mycobacterium tuberculosis*. *Journal of the American Chemical Society*, *126*, 2682–2683.

Sitter, A. J., Shifflett, J. R., & Terner, J. (1988). Resonance Raman spectroscopic evidence for hemeiron-hydroxide ligation in peroxidase alkaline forms. *The Journal of Biological Chemistry*, *263*, 13032–13038.

Smulevich, G., Evangelista-Kirkup, R., English, A., & Spiro, T. G. (1986). Raman and infrared spectra of cytochrome *c* peroxidase-carbon monoxide adducts in alternative conformational states. *Biochemistry*, *25*, 4426–4430.

Smulevich, G., Feis, A., & Howes, B. D. (2005). Fifteen years of Raman spectroscopy of engineered heme containing peroxidases: What have we learned? *Accounts of Chemical Research*, *38*, 433–440.

Smulevich, G., Feis, A., Howes, B. D., & Ivancich, A. (2010). Structure-function relationships among heme peroxidases: New insights from electronic absorption, resonance Raman, and multifrequency electron paramagnetic resonance spectroscopies. In K. M. Kadish, K. M. Smith, & R. Guilard (Eds.), *Handbook of porphyrin science with applications to chemistry, physics, materials science, engineering, biology and medicine: Vol. 6* (pp. 367–455). Singapore: World Scientific.

Smulevich, G., Neri, F., Marzocchi, M. P., & Welinder, K. G. (1996). Versatility of heme coordination demonstrated in a fungal peroxidase. Absorption and resonance Raman studies of *Coprinus cinereus* peroxidase and the Asp245Asn mutant at various pH values. *Biochemistry*, *35*, 10576–10585.

Smulevich, G., Paoli, M., De Sanctis, G., Mantini, A. R., Ascoli, F., & Coletta, M. (1997). Spectroscopic evidence for a conformational transition in horseradish peroxidase at very low pH. *Biochemistry*, *36*, 640–649.

Spiro, T. G. (1982). The resonance Raman spectroscopy of metalloporphyrins and heme proteins. In A. B. P. Lever & H. B. Gray (Eds.), *Iron porphyrins, part II* (pp. 89–152). Reading, MA: Addison-Wesley.

Spiro, T. G. (Ed.), (1988). In *Biological applications of Raman spectroscopy: Resonance Raman spectra of hemes and metalloproteins, Vol. 3*. New York: Wiley.

Spiro, T. G., & Li, X.-Y. (1988). Resonance Raman spectra of metalloproteins. In T. G. Spiro (Ed.), *Biological applications of Raman spectroscopy: Resonance Raman spectra of hemes and metalloproteins: Vol. 3* (pp. 1–37). New York: Wiley.

Spiro, T. G., Soldatova, A. V., & Balakrishnan, G. (2013). CO, NO and O_2 as vibrational probes of heme protein interactions. *Coordination Chemistry Reviews*, *257*, 511–527.

Spiro, T. G., & Wasbotten, I. H. (2005). CO as a vibrational probe of heme protein active sites. *Journal of Inorganic Biochemistry*, *99*, 34–44.

Stein, P., Mitchell, M., & Spiro, T. G. (1980). Hydrogen-bond and deprotonation effects on the resonance Raman iron-imidazole mode in deoxyhemoglobin models: Implications for hemoglobin cooperativity. *Journal of the American Chemical Society*, *102*, 7795–7797.

Streit, B. R., Blanc, B., Lukat-Rodgers, G. S., Rodgers, K. R., & DuBois, J. L. (2010). How active-site protonation state influences the reactivity and ligation of the heme in chlorite dismutase. *Journal of the American Chemical Society*, *132*, 5711–5724.

Teraoka, J., & Kitagawa, T. (1980). Resonance Raman study of the heme-linked ionization in reduced horseradish peroxidase. *Biochemical and Biophysical Research Communications*, *93*, 694–700.

Tinajero-Trejo, M., & Shepherd, M. (2013). The globins of *Campylobacter jejuni*. *Advances in Microbial Physiology*, *63*, 97–145.

Torge, R., Comandini, A., Catacchio, B., Bonamore, A., Botta, B., & Boffi, A. (2009). Peroxidase-like activity of *Thermobifida fusca* hemoglobin: The oxidation of dibenzylbutanolide. *Journal of Molecular Catalysis B: Enzymatic*, *61*, 303–308.

Tsubaki, M., Srivastava, R. B., & Yu, N.-T. (1982). Resonance Raman investigation of carbon monoxide bonding in (carbon monoxy) hemoglobin and -myoglobin: Detection of iron-carbon monoxide stretching and iron-carbon-oxygen bending vibrations and influence of the quaternary structure change. *Biochemistry*, *21*, 1132–1140.

Uno, T., Nishimura, Y., Tsuboi, M., Makino, R., Iizuka, T., & Ishimura, Y. (1987). Two types of conformers with distinct Fe-C-O configuration in the ferrous CO complex of horseradish peroxidase. Resonance Raman and infrared spectroscopic studies with native and deuteroheme-substituted enzymes. *The Journal of Biological Chemistry*, *262*, 4549–4556.

Vinogradov, S. N., Bailly, X., Smith, D. R., Tinajero-Trejo, M., Poole, R. K., & Hoogewijs, D. (2013). Microbial eukaryote globins. *Advances in Microbial Physiology*, *63*, 391–446.

Vinogradov, S. N., & Moens, L. (2008). Diversity of globin function: Enzymatic, transport, storage, and sensing. *The Journal of Biological Chemistry*, *283*, 8773–8777.

Vinogradov, S. N., Tinajero-Trejo, M., Poole, R. K., & Hoogewijs, D. (2013). Bacterial and archaeal globins—A revised perspective. *Biochimica et Biophysica Acta*, *1834*, 1789–1800.

Wainwright, L. M., Wang, Y., Park, S. F., Yeh, S. R., & Poole, R. K. (2006). Purification and spectroscopic characterization of Ctb, a group III truncated hemoglobin implicated in oxygen metabolism in the food-borne pathogen *Campylobacter jejuni*. *Biochemistry*, *45*, 6003–6011.

Wajcman, H., Kiger, L., & Marden, M. C. (2009). Structure and function evolution in the superfamily of globins. *Comptes Rendus Biologies*, *332*(2–3), 273–282.

Wakabayashi, S., Matsubara, H., & Webster, D. A. (1986). Primary sequence of a dimeric bacterial haemoglobin from *Vitreoscilla*. *Nature*, *322*, 481–483.

Wittenberg, J. B., Bolognesi, M., Wittenberg, B. A., & Guertin, M. (2002). Truncated hemoglobins: A new family of hemoglobins widely distributed in bacteria, unicellular eukaryotes, and plants. *The Journal of Biological Chemistry*, *277*, 871–874.

Zhao, H., & Caflisch, A. (2015). Molecular dynamics in drug design. *European Journal of Medicinal Chemistry*, *16*(91C), 4–14.